Commun. Comput. Phys.
doi: 10.4208/cicp.101214.011015a

Vol. **20**, No. 1, pp. 86-135
July 2016

Directly Simulation of Second Order Hyperbolic Systems in Second Order Form via the Regularization Concept

Hassan Yousefi[2,*], Seyed Shahram Ghorashi[3] and Timon Rabczuk[1,4]

[1] *Division of Computational Mechanics, Ton Duc Thang University, Ho Chi Minh City, Viet Nam.*
[2] *Institute of Structural Mechanics, Bauhaus-Universität Weimar, 99423 Weimar, Germany.*
[3] *Research Training Group 1462, Bauhaus-Universität Weimar, 99423 Weimar, Germany.*
[4] *Faculty of Civil Engineering, Ton Duc Thang University, Ho Chi Minh City, Viet Nam.*

Received 10 December 2014; Accepted (in revised version) 1 October 2015

Abstract. We present an efficient and robust method for stress wave propagation problems (second order hyperbolic systems) having discontinuities directly in their second order form. Due to the numerical dispersion around discontinuities and lack of the inherent dissipation in hyperbolic systems, proper simulation of such problems are challenging. The proposed idea is to denoise spurious oscillations by a post-processing stage from solutions obtained from higher-order grid-based methods (e.g., high-order collocation or finite-difference schemes). The denoising is done so that the solutions remain higher-order (here, second order) around discontinuities and are still free from spurious oscillations. For this purpose, improved Tikhonov regularization approach is advised. This means to let data themselves select proper denoised solutions (since there is no pre-assumptions about regularized results). The improved approach can directly be done on uniform or non-uniform sampled data in a way that the regularized results maintenance continuous derivatives up to some desired order. It is shown how to improve the smoothing method so that it remains conservative and has local estimating feature. To confirm effectiveness of the proposed approach, finally, some one and two dimensional examples will be provided. It will be shown how both the numerical (artificial) dispersion and dissipation can be controlled around discontinuous solutions and stochastic-like results.

AMS subject classifications: 35L51, 65N30

Key words: Second order hyperbolic systems, Tikhonov regularization, Numerical (artificial) dispersion.

*Corresponding author. *Email addresses:* hassan.yousefi@uni-weimar.de; hyosefi@ut.ac.ir (H. Yousefi), shahram.ghorashi@uni-weimar.de (S. Sh. Ghorashi), timon.rabczuk@tdt.edu.vn (T. Rabczuk)

1 Introduction

Many high-order numerical schemes (e.g., finite difference, spectral, pseudo-spectral, and finite element methods) have been developed for resolving of elliptic and parabolic partial differential equations (PDEs). This is because, these systems have the inherent dissipation feature [16]. The hyperbolic systems (both the first and second order ones) do not show this inherent feature; even small errors can cause instability in these systems as spurious oscillations [16]. Oscillations in solutions containing discontinuities are known as the numerical dispersion. To remedy this problem, for first-order hyperbolic problems some effective approaches are developed. They include high resolution schemes and discontinuous Galerkin methods (by combining benefits of high-resolution methods with finite elements) [37,58]. In high resolution schemes, in smooth areas higher-order approximations (second, third, or higher ones) are used, and around discontinuities, first order approximation is utilized by a non-linear procedure. This strategy leads to a spurious-oscillation free results.

An effective way for solving second order hyperbolic PDEs is to rewrite them as a system of first order hyperbolic equations and then to simulate them with one of the above-mentioned schemes. This will lead to oscillation free results with small numerical dissipation [32]. The second order hyperbolic PDEs can also be solved in their original second order form. For this purpose, several approaches have been developed:

1. Using artificial dissipation without modifying the governing equations. For this case, dissipation is inherently added in evaluation procedures. In the time domain, the algorithmic dissipative time integration methods have been developed for removing spurious oscillations [20–22, 26]. For the spatial domain, inherent filtering concept is also developed in derivative estimations [69, 70],
2. Adding some artificial viscosity in the governing equations to stabilize the solution. This can be done by using local artificial viscosity around high-gradient zones in the spatial domain [12, 13]. Hughes [25] showed that this approach damps mainly the middle modes without affecting the lower and higher modes substantially. As artificial diffusion decreases accuracy of solutions considerably, methods using the artificial diffusion only in high frequency ranges were developed; such as, the spectral viscosity schemes [8, 9, 56]. This approach has been employed for both first and second order hyperbolic systems,
3. Filtering spurious oscillations from numerical solutions in the spatial domain by a post-processing stage [16, 35]. These schemes were successfully used in simulation of hyperbolic systems on uniform grid points [18, 59, 62], and non-uniform grids [66, 67]. It should be mentioned that many smoothing schemes working satisfactorily on uniform grids are not suitable for non-uniform ones: leading to unstable or unreliable results [39].

The concept of high-resolution treatment has recently been advised for handling second-order hyperbolic systems [3].

The aim of this work is to solve directly the second order hyperbolic systems. Such approach has the following advantages:

1. Less degrees of freedom are needed (in case of elastodynamic problems, in second-order form three dependent variables exist, while between nine and fifteen variables are needed when they are re-formulated as first-order systems);
2. The solution of the first-order system also satisfies the second-order form: this can be done by imposing/checking some constraints. This is because, the first order form admits more acceptable solutions;
3. Possibility of using larger time-steps in second-order form compared to the first-order one [1].

In this work, the spatially filtering approach is used. This will done by a post-processing stage to remove properly spurious oscillations from solutions containing discontinuities. However, curing of the numerical dispersion effects is a crucial task. This is because:

1. Estimation of a function and corresponding derivatives from its sampled points can be considerable as a type of (semi) ill-posed problem. This would be more clear by considering the fact that different estimated values (data and corresponding derivatives) can be obtained for different interpolation methods. From mathematical point of view, this fact may be explainable as follows. Sampling procedure can be considered as convolution of a continuous function $f(x)$ with the Dirac delta $\delta(x)$ as: $f_i=f(x_i)=\int f(x)\delta(x_i-x)\mathrm{d}x$. This integral is known as the first-order Fredholm integral, and corresponding inverse problem could be a (semi) ill-posed problem [19,41], i.e.: finding $f(x)$ from corresponding sampled data $\{f(x_i)\}$;
2. For numerical simulations, it is necessary that derivatives of estimated functions are also to be continuous, or equivalently the derivatives can be properly estimated up to some order. This derivative estimation (from noisy data) is another ill-posed problem. This is because effects of small noise amplify considerably derivative values,
3. Spatial adaptation will insert a new source of ill-posedness; most of filtering methods can not properly work on irregular points/meshes.

Different estimation approaches of functions and their derivatives have been developed; such as: finite-difference methods [31], integral-based schemes [17,33,47,61], regularization approaches [40,60,63], or interpolation methods [28]; for a general overview, the reader is referred to [45,46]. In this work, the regularization approach will be used, where a variational functional is employed. The key challenge is proper handling of the numerical dispersion (known as edge preserving in image processing problems). Therefore, the total variation (TV) based regularization method was developed [53], for preserving discontinuities. Such results, however, are not smooth enough for numerical simulations. Hence, a proper selection of a functional with sufficient smoothness being free from spurious oscillations (due to the numerical dispersion) is important.

In this study, several regularization approaches with different constraints will be studied. Furthermore, effects of imposing extra information containing extra local information will be investigated (it is known as the *model-base* regularization). By using such local extra information, it is tried to impose local features. This extra information is different from the conventional constraints.

These regularization techniques have several advantages over most other denoising schemes; for the Tikhonov method, they are:

1. It has a unique and stable closed-form solution with fast algorithms; this makes it completely popular.
2. It leads to the smoothest possible results for a distinct value of estimation error among all of the regularization schemes.
3. Proper boundary value estimation can be obtained. Estimation errors around boundaries are known as the Runge phenomenon. The Tikhonov regularization method is one of the single-interval schemes that can effectively handle it (without using a anti-Runge scheme) [6,7].
4. Noise can directly be removed from irregularly spaced data where standard filtering techniques used in time series analysis become awkward to implement,
5. By proper selection of prior information, derivatives up to some degree can be estimated,
6. It can deal with many types of ill-posed problems such as data irregularity or derivative estimation problems.

Since the Tikhonov method acts as a post processor, it can be integrated with different explicit/implicit higher-order grid based methods, such as: compact finite difference schemes [35,69,70]. For the Tikhonov-based regularization, other favorable features can also be considered to improve estimated results; such as: conservative regularization (even for non-Gaussian noise), adaptive and/or local(global) smoothing. These extensions for common Tikhonov methods will be presented in this work.

One difficulty in regularization methods is proper choosing of regularization parameters. Indeed, most of the existing estimating methods lead to over or under smoothing results [27,36]. Current experiments reveal that even small amount of regularization can considerably improve numerical results. In general, the trial-and-error method can be recommended to find an optimum range of regularization parameters. Error bounds and convergence rates are studied for commonly used constraints or regularization definitions; e.g., see: [2, 44]. Here, for recently proposed constraint in [30] for the Tikhonov method, error bounds and convergence rates are also studied.

This paper is organized as follows. Section 2 describes the main concept of regularization. Regularization-based numerical solutions of 1D stress wave propagation problems containing discontinuities are studied in Section 3. In Section 4, the explicit/implicit higher order finite difference methods are explained with corresponding filtering algorithms. In this section, the Tikhonov-based smoothing will be integrated with such higher-order methods. The performance of this collaboration will be studied by both

smooth and discontinuous solutions. In Section 5, by using the singular value decomposition (SVD) and the generalized one (GSVD), effects of different constraints for the Tikhonov method are studied. The implementation of the Tikhonov method with different constraints are presented in Section 6. In Section 7, error estimations and convergence rates are investigated. These concepts are then studied by a benchmark having a discontinuity; there, both of the numerical dispersion and Runge phenomenon are investigated. Section 8 devotes to the conservative filtering feature in the Tikhonov method. In Section 9, it will be shown how to have a local smoothing with Tikhonov methods by considering extra constraints. Relationship between Tikhonov-based smoothing methods and classical filtering concepts in signal processing schemes will be explained in Section 10. Section 11 discusses general algorithms for the numerical simulation of second-order hyperbolic systems. Some examples in finite and infinite-periodic domains with fixed and absorbing boundary conditions are tested in Section 12; here, effects of the numerical dispersion and artificial dissipation are studied. The paper ends with a brief conclusion.

2 Regularization approaches

2.1 Tikhonov regularization method with different constraints

The aim of regularization is to replace an ill-posed problem with a nearly well posed one. Let assume uniformly sampled (noisy) data $\{\{y_i\}; i\in\{1,2,\cdots,n\}\}$; to have a stable estimation of smoothed (denoised) data $\{\{f_j\}; j\in\{1,\cdots,n\}\}$ from $\{y_i\}$, a functional Q resulted from a linear combination of the residual norm $\rho(\mathbf{y}-\mathbf{f})=\|\mathbf{y}-\mathbf{f}\|_2=\sqrt{\sum_{i=1}^{n}(y_i-f_i)^2}$ and prior information $\Omega(\mathbf{f})$ is considered, as [19,41]:

$$Q(\mathbf{f})=\rho(\mathbf{y}-\mathbf{f})^2+\lambda\times\Omega(\mathbf{f})^2, \tag{2.1}$$

where λ $(0\leq\lambda<\infty)$ is a penalization factor. The solution $\{f_j\}$ minimize this functional. Parameter λ controls trade-off between error in estimations and smoothness. The cases $\lambda\to 0$ and $\lambda\to\infty$ lead to the linear fit and interpolation problems, respectively. Taking advantage of the remapping relation $\lambda=(1-p)/p$, the range of λ can be changed to $[0,1]$; $p=1$ results in an interpolation problem, and lower values yield more smoother estimations. It should be mentioned that the commonly used Tikhonov formulation can slightly be modified, for example as: $Q(\mathbf{f})=\rho(\mathbf{y}-\mathbf{f})^2+(\int f(x)\mathrm{d}x)^2+\lambda\times(\|\mathbf{f}\|^2+\|\mathbf{f}'\|^2)$ (where $\mathbf{f}':=\mathrm{d}\mathbf{f}/\mathrm{d}x$) [11].

The stationary point of $Q(\mathbf{f})$ is the minimizing solution: $\mathbf{f}_{min}=\mathrm{argmin}_{\mathbf{f}}(Q(\mathbf{f}))$. Some constraints $\Omega^2(\mathbf{f})$ with corresponding features are briefly reviewed in Table 1. There, constraints with and without models (prior extra information) are presented.

The model-based Tikhonov regularization was introduced by Barakat et al. [4]. It introduces extra information f_{model} (containing generally localized information) to improve regularization. The modified constraint (measured usually by a (semi) norm) is: $\Omega^2_{model}=\|D^{(m)}(f-f_{model})\|_2^2$ (where $D^{(m)}$ denotes an operator for m^{th} derivative). If

Table 1: Different constraint definitions in the L_2 space for the Tikhonov method.

Constraint	Feature
$\Omega_0^2(x)=\int_{-\infty}^{+\infty}(f'(x))^2\mathrm{d}x$,	Using a smoothness constraint: having first order continuity [24],
$\Omega_1^2(x)=\int_{-\infty}^{+\infty}(f''(x))^2\mathrm{d}x$,	Using a smoothness constraint: having second order continuity and a physical meaning. It measures flexural energy in a beam [19,41],
$\Omega_2^2(x)=\int_{-\infty}^{+\infty}(f''(x)+\alpha f'(x))^2\mathrm{d}x$,	Using a smoothness constraint: regularized solutions have second order continuity. This definition was recently proposed [30]. It leads to smoothing splines in tension,
$\Omega_3^2(x)=\int_{-\infty}^{+\infty}(f''(x)^2+\alpha^2 f'(x)^2)\mathrm{d}x$,	Using a smoothness constraint: regularized solutions have second order continuity. This leads to smoothing splines in tension. This definition has a physical meaning: it measures energies of flexural and axial deformations in a beam [42,43,48,49],
$\Omega_{model}^2(x)=\|D^{(m)}(f-f_{model})\|_2^2$; $m\in\{0,1,2\}$,	The model-based regularization by using extra prior information f_{model}; it can include several locally imposed features [4],
$\Omega_4^2(x)=\int_{-\infty}^{+\infty}(\lvert f'(x)+1\rvert-1)^2\mathrm{d}x$,	Area (or volume) preserving constraint [51].

the model f_{model} is properly chosen, this modification will lead to a good estimation. For example, if f_{model} has some discontinuities, this local information of signal can be used in regularization procedures. Even though, the Tikhonov method leads to unique and stable solutions, prior general information like bounded smoothness is not often enough to obtain a suitable solution due to a global character. It will be shown that model-based regularized solutions are also sensitive to the model, itself. This sensitivity is due to existence of high-frequency components in systems. This will be confirmed by the GSVD in Section 5.

The Tikhonov regularization method leads to a closed form solution. However, the main disadvantage of the Tikhonov method is that it cannot properly handle discontinuities in a considered system.

All of the above mentioned constraints are defined in the L_2 space; there exists some other effective constraints which measure prior information in L_1 space (e.g., with (semi) norm $\int(\lvert f^{(m)}(x)\rvert\mathrm{d}x$, $m\geq 0$; where $f^{(m)}:=\mathrm{d}^m f/\mathrm{d}x^m$). They are developed to handle special problems, like the edge preserving restoration (preserving discontinuity). In this case, the functional Q can generally be defined as: $Q(\mathbf{f})=\rho(\mathbf{y}-\mathbf{f})^2+\lambda\times\Omega(\mathbf{f})$. Some of such constraint definitions are: 1) the Total Variations (TV) [53]; 2) the incompressibility; 3) local rigidity [52]. For these regularization methods, closed-form solutions can not be provided; they are mainly solved by iterative algorithms.

As mentioned, the main shortcoming of the Tikhonov method is proper handling of

discontinuities. The TV-based regularization is originally developed to preserve image edges or data discontinuities. Corresponding constraint can be defined as: $\Omega_{TV}(f) = \int_{-\infty}^{+\infty} |f^{(m)}(x)| \mathrm{d}x$, $m \in \{0,1\}$. Regarding numerical simulations, however, the authors experience shows that this approach does not have enough smoothness; this makes it unsuitable for PDE solutions (this will be studied).

Some remarks: considering above mentioned methods, it should be noted that:

1. In the above-mentioned regularization methods, it is assumed that the noise has the white Gaussian feature. This means, the discrete values $y_i := y(x_i)$ can be written as: $y_i = f_i + \epsilon_i$; where $i \in \{1,2,\cdots,n\}$; $x_1 \leq x_2 \leq \cdots \leq x_n$; $\{\epsilon_i\}$ are random, uncorrelated errors with zero mean and variance σ^2; $f(x)$ is the denoised (smooth) function which should be estimated.
2. For other types of noise, different modified definitions should be used. For the Poisson noise see, e.g. [34], and for general cases, see [10, 50].
3. Regarding several regularization constraints, it has been noted that their effects can be viewed as a high-pass filter [5, 15]. This will be shown in Sec. 10.

2.2 Curing discontinuity effects: the numerical dispersion around discontinuities

To handle properly discontinuities in regularization problems, several approaches are proposed; some of which are:

1. The common Tikhonov method (using common smoothness constraints, e.g.: Ω_1^2) with adaptive weight coefficients [57]. In this approach, The aim is to estimate a function with different smoothness in different spatial locations. However, discontinuity types and corresponding locations should be known, as prior information. This makes this approach, in general, unfeasible.
2. Using a smoothness constraint having a tension term (i.e., Ω_2^2 and Ω_3^2) in the Tikhonov approach,
3. The TV-based regularization,
4. The model-based Tikhonov regularization.

The first, second and fourth approaches have closed-form solutions with fast algorithms; this makes such methods appealing for numerical simulation of boundary value problems. The third approach can effectively handle discontinuities. However, it suffers from lack of smoothness and utilizing of iterative solvers.

2.3 2D regularization methods

Extension of 1D regularization definitions to higher-dimension problems are straightforward: the same concepts and measurements can be used, as well. For example, for the Tikhonov method with a smoothness constraint (if the smoothness is measured by the gradient constraint, like Ω_0^2 in the 1D case), the corresponding functional can be written as: $Q=\int_\Omega (z(x,y)-f)^2 \mathrm{d}\Omega+\lambda\int_\Omega |\nabla f|_2^2 \mathrm{d}\Omega$ (where $|\nabla f|_2^2:=\{D_x(f)^2+D_y(f)^2\}$, where the operator D_i is the first derivative definition in the i^{th} direction and $i\in\{x,y\}$).

In this work, to have a cost-effective algorithm, higher-order problems are solved based on 1D algorithms. For this purpose, firstly, in each direction, 1D algorithms are independently implemented, and then average of results are considered as a regularized solution. This means, for spatial point (x_i,y_j), the approximated solution is: $f(x_i,y_j)=0.5(f_1(x_i)+f_2(y_j))$, where f_1 and f_2 are the regularized solutions obtained independently in the x and y directions, respectively.

3 Numerical simulation of 1D wave problems via regularization methods

In this section, 1D wave propagation problems including (semi) discontinuities will be studied to reveal effectiveness of different regularization approaches. The problem is longitudinal wave propagation in a bar with a constant cross section area. The governing equation is: $\partial^2 u(x,t)/\partial t^2=c^2\partial^2 u(x,t)/\partial x^2:\ 0\le x\le 1$; the initial (ICs) and boundary (BCs) conditions are $\{u(x,t=0)=u_0\ \&\ \dot{u}(x,t=0)=v_0\}$ and $\{u(0,t)=u(1,t)=0\}$, respectively (where $\dot{u}:=du/dt$). Here u denotes the axial deformation and c is the wave propagation speed. The velocity c is assumed to be $c=\sqrt{E/\rho}=1$; where E and ρ are the module of elasticity and density of the bar, respectively.

For numerical simulations, in spatial domain, the higher-order finite difference method is used: the fourth-order explicit central difference approximation for the second derivative. The temporal integration is done with the Runge-Kutta 4^{th} order method, see Appendix A. For spatio-temporal discretizations, it is assumed: $dx=1/2^9$ and $dt=10^{-8}$. After each five time steps, numerical solutions are regularized (denoised) with different regularization approaches (as a post-processor).

Several different imposed initial displacements will be considered; both smooth but high gradient deformations and those having discontinuities. The considered ICs for u_0 are:

1. $u^{(1)}(x,t=0)=u_0^{(1)}=\sqrt{\max(1-(\frac{x-x_c}{0.5\times Supp})^2,0)}$, where x_c and $supp$ are center point and support length of the function, respectively. Here, it is assumed: $x_c=0.5$ and $supp=0.2$,
2. A dilated unit box with definition: $u^{(2)}(x,t=0)=u_0^{(2)}=\text{UnitBox}(4(x-0.5))$, where $\text{UnitBox}(x)=H(x+0.5)-H(x-0.5)$; the function $H(x)$ is the Heaviside function,

3. A compact sawtooth wave function: $u^{(3)}(x,t=0)=u_0^{(3)}=\text{UnitBox}(\frac{(x-x_c)}{supp})(x-x_c+0.5)\times supp$, where $x_c=0.5$ and $supp=0.2$.

In all cases, it is assumed $v_0=0$.

In the following, numerical results of the wave propagation problem will be studied; they are resulted from different regularization/constraint definitions.

Numerical results from the Tikhonov method with different constraints and without a model

For regularization stage, penalizing (smoothing) parameter is assumed to be: p=0.875 and $\alpha=1$. Numerical results, denoised by the Tikhonov method with constraints Ω_1^2, Ω_2^2 and Ω_3^2, are shown in Fig. 1. The constraint Ω_1^2 is a commonly used smoothness-based regularization, and the Ω_2^2 and Ω_3^2 are those improved by considering a tension term (see Table 1). Adding this term helps to reduce undesirable fluctuations from fitted curves. The constraint Ω_3^2 are widely used, and the Ω_2^2 is recently recommended (see Table 1). Based on the results, it is clear that, even though both of constraints Ω_2^2 and Ω_3^2 use the concept of tensioned curves, in all cases the constraint Ω_2^2 can effectively control the numerical dispersion.

The model-based Tikhonov regularization

In the following, effects of the model-based Tikhonov regularization approach will be studied by some numerical simulations. The considered constraints for obtaining $\mathbf{f}_{min}$ are: Ω_1^2, Ω_2^2 & Ω_3^2. To estimate $\mathbf{f}_{model}$, a regularization problem is firstly solved at each denoising stage; for this reason, the Tikhonov method with constraints Ω_1^2, Ω_2^2 & Ω_3^2 are used. The $\mathbf{f}_{model}$ is also estimated with the TV regularization approach. Regarding the wave propagation problem, the results are presented in Fig. 2 with IC $u^{(1)}(x,t=0)$ at $t=0.2$ (simulation of smooth but high-gradient solutions). There, in figures (a) to (f), for $\mathbf{f}_{model}$ and $\mathbf{f}_{min}$, the following constraints are considered: {figure (a): for f_{model}: Ω_1^2 & for f_{min}: Ω_1^2}; {figure (b): for f_{model}: Ω_2^2 & for f_{min}: Ω_2^2}; {figure (c): for f_{model}: Ω_3^2 & for f_{min}: Ω_3^2}; {figure (d): for f_{model}: Ω_{TV}^2 & for f_{min}: Ω_1^2}; {figure (e): for f_{model}: Ω_{TV}^2 & for f_{min}: Ω_2^2}; {figure (f): for f_{model}: Ω_{TV}^2 & for f_{min}: Ω_3^2}.

It is clear that in all cases spurious oscillations exist, and the model-based regularization can not effectively control the numerical dispersion. This is due to amplification of high-frequency components in the system (this will be shown). This shortcoming is more highlighted in discontinuous cases. To study this, the wave propagation problem with initial condition $u^{(2)}(x,t=0)$ is considered. The corresponding results are represented in Fig. 3 with the same assumptions of Fig. 2. It is obvious that effects of spurious oscillations are considerable in this case. This is due to existence of more high frequency components in this system in comparison to the previous smooth high-gradient solutions.

To study estimation errors in different regularization approaches, the L-curves of solutions are also presented. The L-curve is a graphical log-log representation of a constraint Ω^2 (or Ω_{TV}^2) against the estimation error ρ_2^2. Regarding the 1D wave propagation

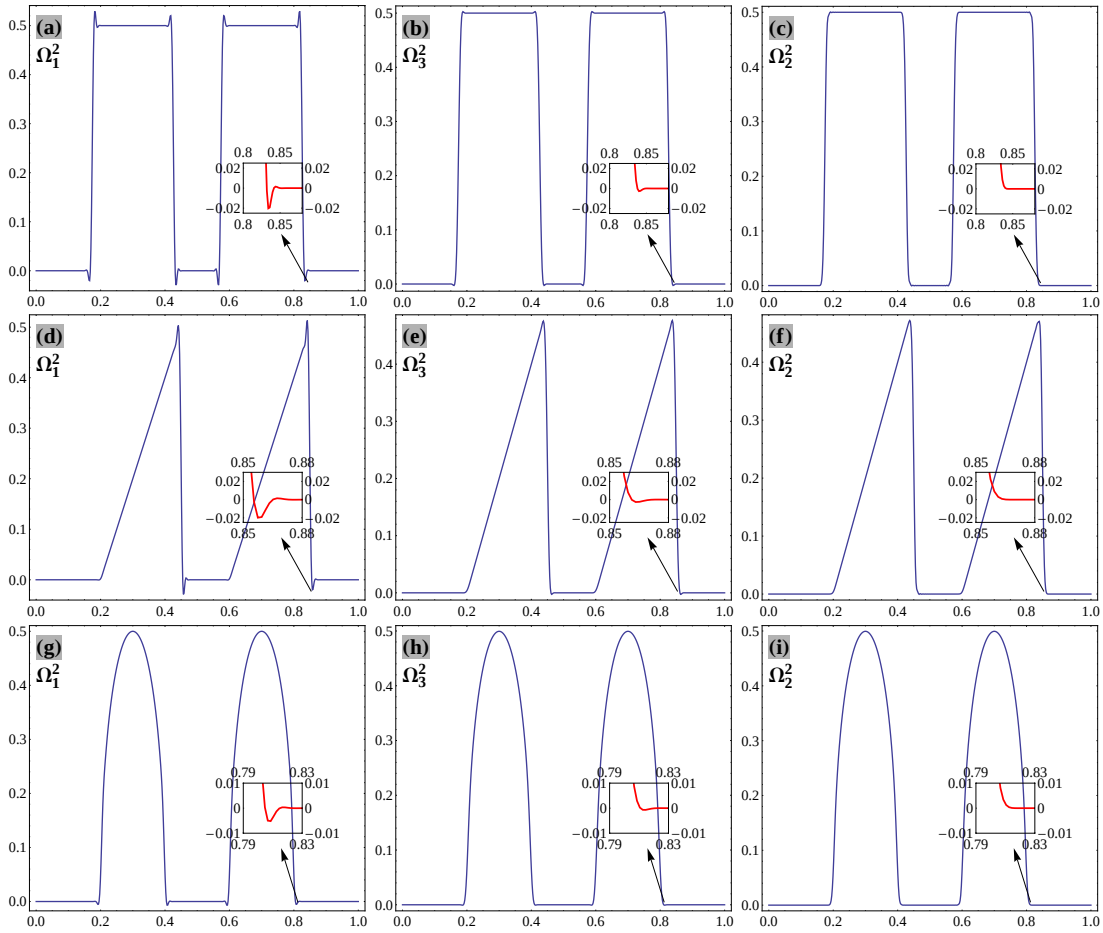

Figure 1: Numerical solutions with different Tikhonov methods with parameters $p=0.875$ and $\alpha=1$ at $t=0.2$. The numerical dispersion appears in solutions obtained by the constraints Ω_1^2 and Ω_3^2.

problem, for the smooth-high gradient IC ($u^{(1)}(x,t=0)$), corresponding L-curves are presented in Fig. 4. In the simulations, different regularization parameters are assumed, as: $p\in\{0.65,0.7,0.73,0.75,0.8,0.85,0.9,0.92,0.94,0.96,0.98,0.99\}$. The results are for time $t=0.2$.

In figure (a), the L-curve of numerical solutions obtained by the Tikhonov-based filtering are compared with each other; the considered constraints are: Ω_1^2, Ω_2^2, and Ω_3^2. It is clear that the common Tikhonov method (using Ω_1^2) leads to the smoothest possible result. By using the two other constraints, at the expense of error in estimations, smoother results can be obtained. Also Ω_2^2 constraint leads to slightly smoother results than those of Ω_3^2. In figure (b) TV-based results are compared with those obtained by the common Tikhonov scheme; it is obvious, the TV-based results lead to worse results (this is due to lack of enough-smoothness). Finally, in figure (c), the common Tikhonov method with and without the model are compared with each other; for the model-based filtering, the

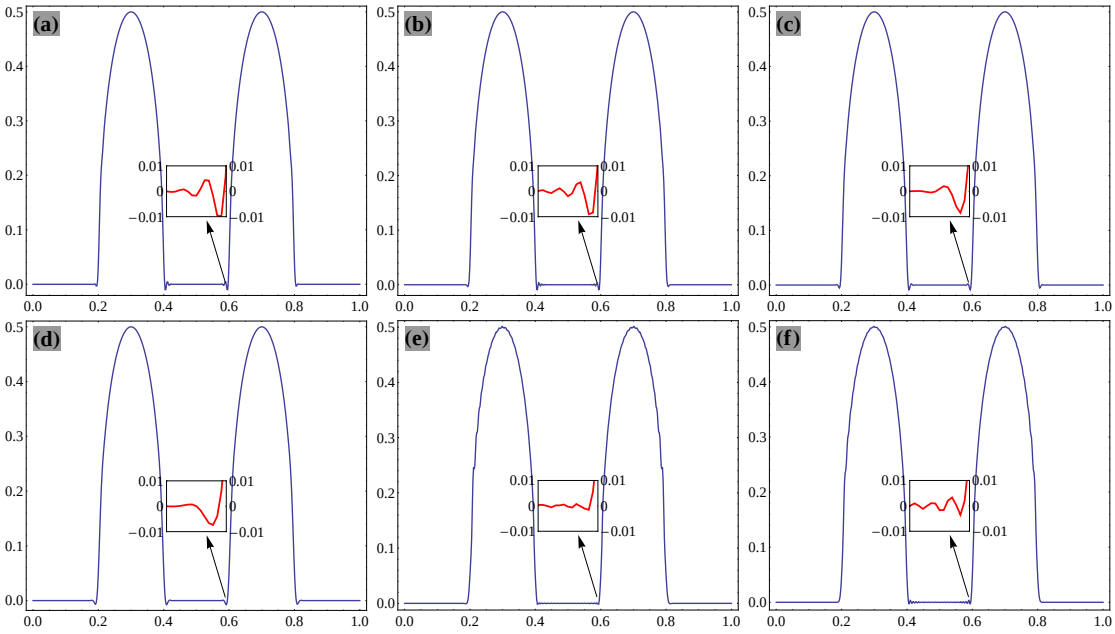

Figure 2: Numerical solutions of the wave propagation problem, denoised with the model-based Tikhonov scheme with constraints Ω_1^2, Ω_2^2 & Ω_3^2 at $t=0.2$; for each figure, for pair $\{\mathbf{f}_{model},\mathbf{f}_{min}\}$, corresponding constraint pairs are: a) $\{\Omega_1^2,\Omega_1^2\}$; b) $\{\Omega_2^2,\Omega_2^2\}$, c) $\{\Omega_3^2,\Omega_3^2\}$, d) $\{\Omega_{TV}^2,\Omega_1^2\}$, e) $\{\Omega_{TV}^2,\Omega_2^2\}$, f) $\{\Omega_{TV}^2,\Omega_3^2\}$.

constraint pair $\{\mathbf{f}_{model},\mathbf{f}_{min}\}=\{\Omega_1^2,\Omega_1^2\}$ is used. In the model-based Tikhonov regularization, smooth solutions are only obtained for small p values; this is due to presence of small oscillations in over-smoothed regularized solutions (as seen before).

4 Higher order finite difference methods and different filtering approaches

Considering linear wave propagation problems, two general higher-order differencing approaches will be reviewed in this section. The approaches are: 1) those using inherent filtering; 2) ones utilizing filters by a post-processing stage. In the former case, spatial filtering can inherently be considered in corresponding formulations. Performance of these two approaches would then be studied for both smooth-high gradient and discontinuous solutions. Below, above-mentioned approaches and corresponding filters are reviewed.

4.1 Approach 1: Inherent filtering

Here, filtering effects are inserted in definition of spatial derivatives. This inserting can be done to have either a maximum order of accuracy or some optimized quantities [69,70].

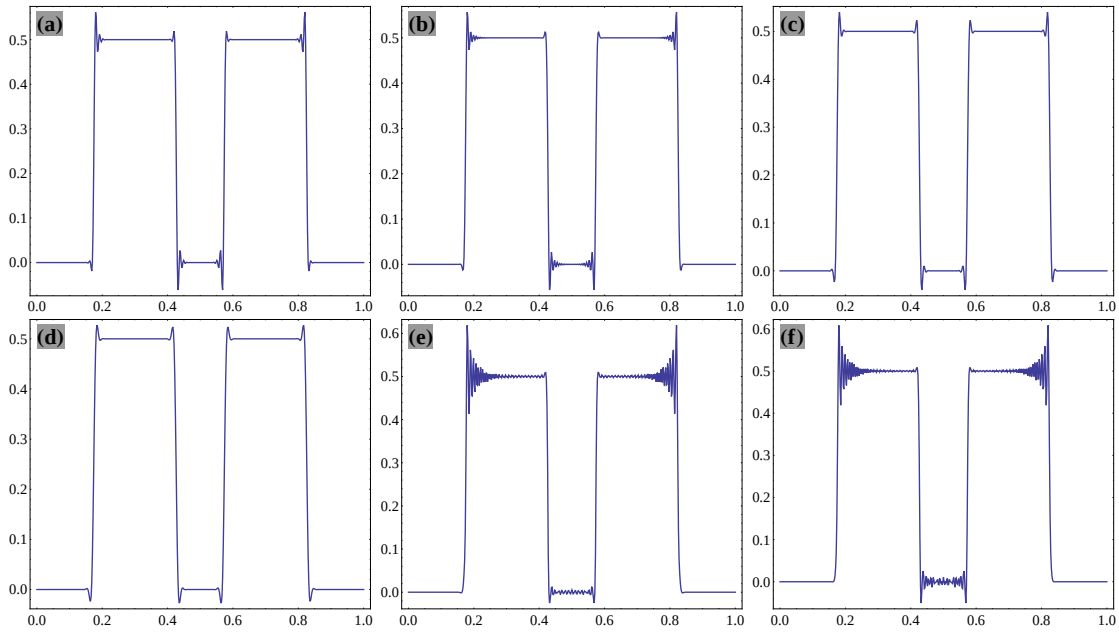

Figure 3: Numerical solutions of the wave propagation problem having discontinuous fronts, denoised with the model-based Tikhonov scheme with constraints Ω_1^2, Ω_2^2 & Ω_3^2 at $t=0.2$; for each figure, for the pair $\{\mathbf{f}_{model},\mathbf{f}_{min}\}$, corresponding constraints are: a) $\{\Omega_1^2,\Omega_1^2\}$; b) $\{\Omega_2^2,\Omega_2^2\}$, c) $\{\Omega_3^2,\Omega_3^2\}$, d) $\{\Omega_{TV}^2,\Omega_1^2\}$, e) $\{\Omega_{TV}^2,\Omega_2^2\}$, f) $\{\Omega_{TV}^2,\Omega_3^2\}$.

4.1.1 Maximum order schemes

In this approach, order of accuracy is maximized by considering error terms. For a uniform grid $x_j := j\,\Delta x$, at point x_j, the first spatial derivative can be approximated as:

$$(\delta_x u)_j = \frac{1}{\Delta x}\{(d_3-a_3)u_{j-3}+(d_2-a_2)u_{j-2}+(d_1-a_1)u_{j-1}+d_0u_j \\ +(d_1+a_1)u_{j+1}+(d_2+a_2)u_{j+2}+(d_3+a_3)u_{j+3}\}, \tag{4.1}$$

where: $u_j := u(x_j)$; $(\delta_x u)_j := \mathrm{d}(u(x_j))/\mathrm{d}x$; a_i and d_i are coefficients of anti-symmetric ($(\delta_x^a u)_j$) and symmetric ($(\delta_x^s u)_j$) parts, respectively. The symmetric part, $(\delta_x^s u)_j$ acts as a spatial filter. The maximum order of accuracy for $(\delta_x u)_j$ without and with filtering effects ($(\delta_x^s u)_j$) are six and five, respectively. For the six-order accuracy, the coefficients are: $a_1=3/4$, $a_2=-3/20$, $a_3=1/60$, $d_1=d_2=d_3=0$; and for the five-order one, the set $\{d_i\}$ becomes: $d_1=-3d_0/4$, $d_2=3d_0/10$, and $d_3=-d_0/20$. In our study, it is assumed: $d_0=0.1$ [69].

Regarding a system of pure advection, $\mathbf{u}_t+(\mathbf{Au})_x=\mathbf{0}$ (where, $\mathbf{u}_t:=\mathrm{d}\mathbf{u}/\mathrm{d}t$ and $(\mathbf{Au})_x:=\mathrm{d}(\mathbf{Au})/\mathrm{d}x$), the spatial first derivative of the flux $(\mathbf{Au})$ can be approximated as:

$$(\mathbf{Au})_x \approx \delta_x^a\mathbf{Au}+\delta_x^s|\mathbf{A}|\mathbf{u}, \tag{4.2}$$

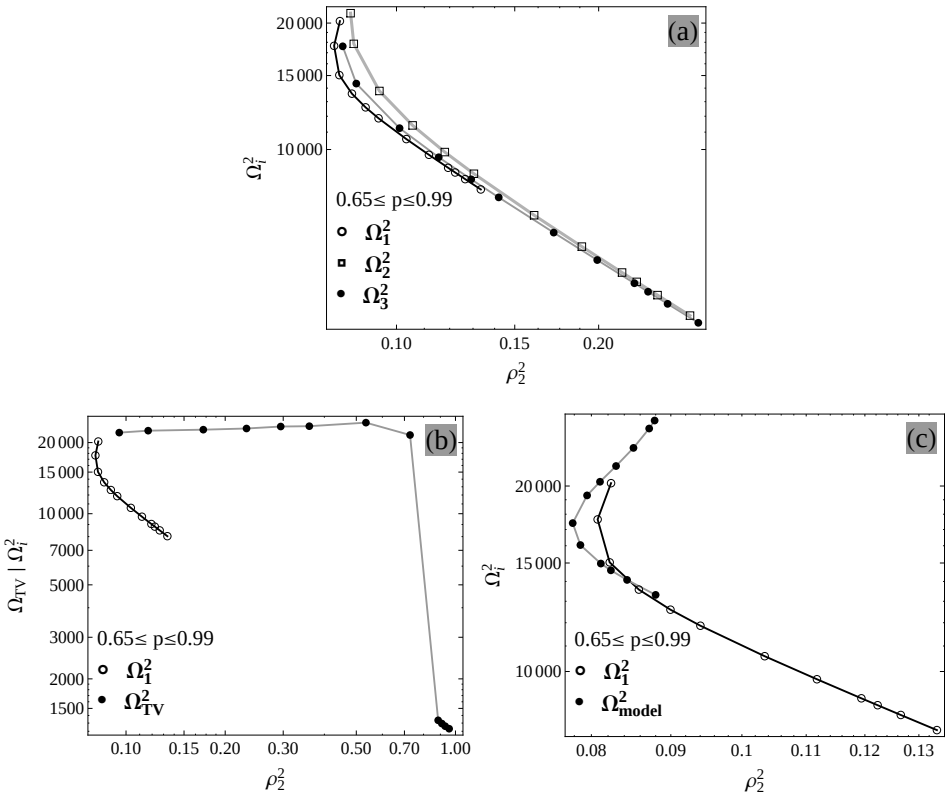

Figure 4: The L-curves for numerical solutions of the 1D wave propagation problem at $t=0.2$, denoised with different regularization approaches.

where: $|\mathbf{A}|=\mathbf{X}|\boldsymbol{\Lambda}|\mathbf{X}^{-1}$. Matrices $\mathbf{X}$ and $\boldsymbol{\Lambda}$ denote right eigenvectors and eigenvalues of $\mathbf{A}$, respectively.

Temporal integration of the advection equation can be done by the six stage explicit method mentioned in [69], as:

$$u_{n+\alpha_i}^{(i)}=u_n+\Delta t\alpha_i f_{n+\alpha_{i-1}}^{(i-1)},\quad \text{for}\quad i=\{1,2,\cdots,6\}, \tag{4.3}$$

where: i denotes integration stage; $\alpha_0=0$, and $\alpha_6=1$; $f_n^{(0)}=f_n$; $u_{n+\alpha_6}^{(6)}=u_{n+1}$; $u_n:=u(t_n)$; $f^{(k)}:=du^{(k)}/dt$. To have a six-order temporal accuracy, in case of linear homogeneous ordinary differential equations (ODEs), the set $\{\alpha_i\}$ should be: $\alpha_1=1/6$, $\alpha_2=1/5$, $\alpha_3=1/4$, $\alpha_4=1/3$ and $\alpha_5=1/2$.

4.1.2 The optimized method

Definition of $(\delta_x u)_j$ (from Eq. (4.1)) with filtering effects and six-stage temporal integration (Eq. (4.3)) can be optimized for some desire error behavior or requirements. To resolve more waves of larger wave numbers (or short waves), corresponding optimized

solution can be obtained in spatio-temporal domains by coefficients: $a_1 = 0.7599613$, $a_2 = -0.1581220$, $a_3 = 0.01876090$, $d_1 = -0.07638461$, $d_2 = 0.03228961$, $d_3 = -0.005904994$, $\alpha_1 = 0.168850$, $\alpha_2 = 0.197348$, $\alpha_3 = 0.250038$, $\alpha_4 = 0.333306$, $\alpha_5 = 0.5$ [69,70].

4.2 Approach 2: Post-processing based filtering

In this approach, at first, derivatives or solutions are obtained and then by a post-processing stage, non-physical oscillations are removed from numerical solutions. In the following, generalized compact finite difference schemes with different features and a general filtering method are reviewed.

4.2.1 Compact finite difference schemes

In this approach, a linear combination of data values $\{u_i\}$ are locally used for estimation of derivatives values in each grid point. This combination for the first and second derivatives can be written as [35]:

$$\beta_m u_{i-2}^{(m)} + \alpha_m u_{i-1}^{(m)} + u_i^{(m)} + \alpha_m u_{i+1}^{(m)} + \beta_m u_{i+2}^{(m)} = c_m Z_{i,3}^{(m)} + b_m Z_{i,2}^{(m)} + a_m Z_{i,1}^{(m)}, \quad \text{for} \quad m \in \{1,2\}, \tag{4.4}$$

where: $Z_{i,j}^{(1)} := \frac{u_{i+j} - u_{i-j}}{2(j\Delta x)}$; $Z_{i,j}^{(2)} := \frac{u_{i+j} - 2u_i + u_{i-j}}{(j\Delta x)^2}$; and $u_i^{(m)} := d^m u_i / dx^m$. Eq. (4.4) is also known as the generalized Padé scheme. Relationships between coefficients $\{a_m, b_m, c_m\}$ and $\{\alpha_m, \beta_m\}$ can be obtained by matching the Taylor series coefficients. The truncation error can be obtained by the first un-matched coefficient. The coefficients $\{a_m, b_m, c_m\}$ and $\{\alpha_m, \beta_m\}$ for case $m = 2$ (i.e., the second derivative) with periodic boundary conditions are presented in Table 2 for different spatial accuracy [35]. For estimation of the first and second derivatives on a domain with general boundary conditions, please see [35].

Noise can be filtered by a post-processing stage in the spatial domain; following the idea of local differencing, filtered data can be estimated as [35]:

$$\widehat{\beta}\hat{u}_{i-2} + \widehat{\alpha}\hat{u}_{i-1} + \hat{u}_i + \widehat{\alpha}\hat{u}_{i+1} + \widehat{\beta}\hat{u}_{i+2} = \widehat{d}\hat{Z}_{i,3} + \widehat{c}\hat{Z}_{i,2} + \widehat{b}\hat{Z}_{i,1} + \widehat{a}\hat{Z}_{i,0}, \tag{4.5}$$

where: $\hat{Z}_{i,j} := (u_{i+j} + u_{i-j})/2$; and $\{\hat{u}_i\}$ denotes the filtered data at grid points $\{x_i\}$. The coefficients $\{\widehat{a}, \widehat{b}, \widehat{c}, \widehat{d}\}$ and $\{\widehat{\alpha}, \widehat{\beta}\}$ are presented in Table 3 for the periodic boundary condition and for different accuracy.

4.3 Performance of two approaches for smooth and discontinuous solutions

Below, performance of two approaches (1) and (2) will be studied for both smooth and discontinuous solutions by a 1D scalar stress wave propagation problem. There, effects of different filtering methods, inherent and post-processing ones, will be considered. In case of the post-processing approach, effects of Tikhonov-based smoothing (regularization) will also be studied.

The example is a wave propagation problem in an elastic bar with unit length, unit wave-propagation velocity (c=1) and periodic boundaries. The problem is only subjected to an imposed initial displacement $u_0(x)$ ($v_0(x)$=0). Two different smooth and discontinuous initial displacements are considered respectively, as: $u_0(x)$:=Exp$(-500(x-0.5)^2)$, and $u_0(x)$:=Unitbox$(4(x-0.5))$ for $0\leq x\leq 1$.

In numerical simulations, it is assumed:

1. both the l_2 and l_1 norms are used to measure errors; error definitions for l_2 and l_1 norms are $\|e\|_2:=\frac{1}{N_g}\{\sum_{i=1}^{N_g}(u_i-u_i^{ex})^2\}^{1/2}$ and $\|e\|_1:=\frac{1}{N_g}\sum_{i=1}^{N_g}|u_i-u_i^{ex}|$, respectively; where $u_i:=u(x_i)$; u^{ex} denotes the exact solution; and N_g shows number of grid points,
2. for the time integration, the Runge-Kutta 4^{th} order is used for the explicit 4^{th} order (4-C) and the Padé differencing schemes (4-P) (see Table 2); the 6^{th} order, six stage temporal integration (Eq. (4.3)) is used for remaining spatial differencing operators [70],
3. in all simulations, a fixed Courant number, $C_{CFL}:=c\,\Delta t/\Delta x$ (known as the CFL condition) is used, as: $C_{CFL}=1/3$,
4. smoothing is done at each time step (for both inherent and post-processing approaches).

Convergence rates are studied in Fig. 5 for both smooth and discontinuous solutions at $t=0.2$; slope of lines are measured as $1:(-v)$ (i.e.: 1 and $(-v)$ units in the horizontal and vertical directions, respectively). In this figure, the top and bottom rows belong to the smooth and discontinuous solutions, respectively. Fig. 5(a) corresponds to the generalized Padé schemes without filtering stage. The filtered results (by a post-processor) are represented in Fig. 5(b) for two different filters: the 6^{th} order explicit ("f-6-E") and 4^{th} order implicit pentadiagonal ("f-4-p-1") methods (see Table 3). In Fig. 5(c), the results belong to the inherent filtering approach; here, the 6^{th} order method (Max order-6^{th}) does not use any filters. Fig. 5(d) is for the generalized Padé schemes using the Tikhonov-based smoothing with constraints Ω_1^2 and Ω_2^2 (with parameters: $p=0.99$ and $\alpha=0.99$). For the discontinuous solution, all of the results are re-presented in Figs. 5(e)- 5(g). The post-processing (Eq. (4.5)), inherent (Eq. (4.1)) and Tikhonov-based filtering are used for denoising compact difference schemes and their results are presented respectively in Figs. 5(e), 5(f) and 5(g). The results offer that: 1) in smooth solutions (Fig. 5(a)), predicted convergence rates can be obtained (except for the 10^{th} order one where it seems that a more accurate time integration method should be used); 2) filtering changes convergence rates and this is considerable for discontinuous solutions; in this case, the rates are generally less than one; 3) regarding discontinuous solutions, for the inherent filtering approach, performance of optimized methods is better than those of the maximum order schemes; this is because, optimized methods can detect more waves of large wave numbers (this will be clarified); 4) in smooth solutions, performance of the Tikhonov method

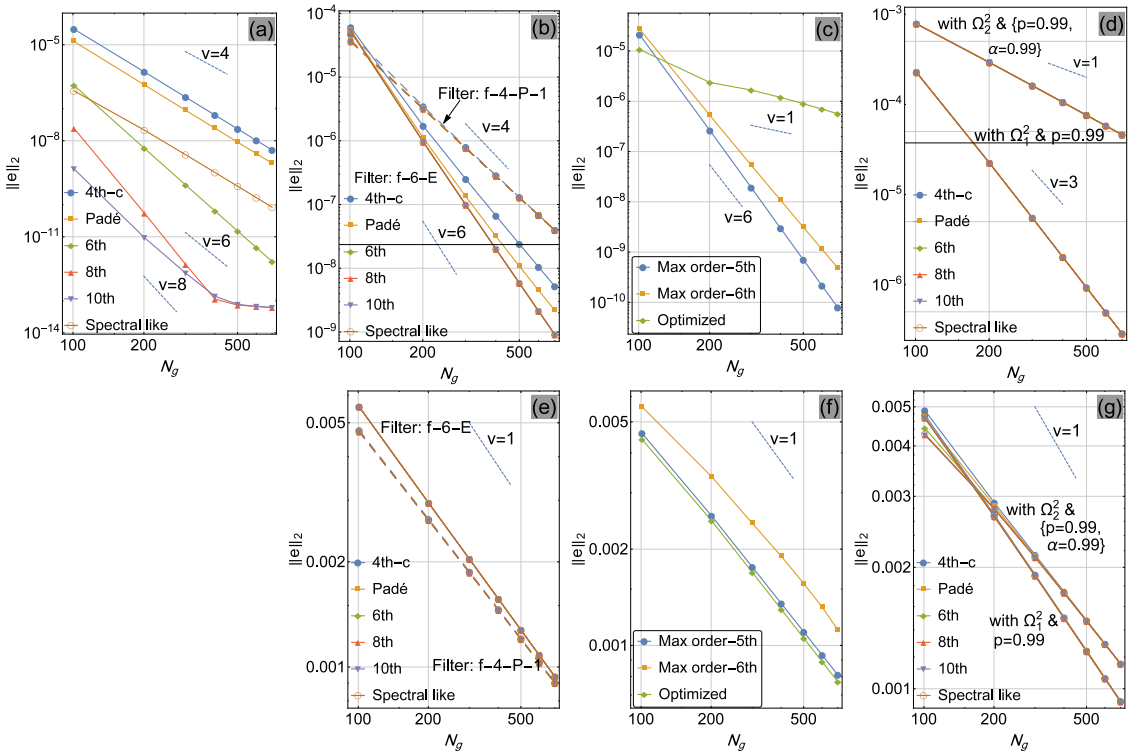

Figure 5: Convergence rates in the l_2 norm for different FD methods for smooth (top row) and discontinuous (bottom row) solutions; a) different compact FDs without filtering; b, e) different compact FDs with filtering; c,f) the inherent filtering approach; d,g) Tikhonov based smoothing by a post-processor stage.

with the constraint Ω_1^2 is better than those with the constraint Ω_2^2; however in discontinuous solutions, the Ω_2^2 constraint can control the numerical dispersion more effectively and can prevent the numerical dispersion (will be studied).

Convergence rates in the l_1 norm is also presented for the discontinuous solutions in Fig. 6. It is clear that convergence rates are less than one for the all cases.

To clarify filtering effectiveness (for controlling the numerical dispersion and dissipation phenomena), solutions $u(x,t=0.2)$ are presented in Fig. 7 for different FD methods and filtering approaches. It is clear that the Tikhonov method with constraint Ω_2^2 can properly be integrated with other differencing schemes to control the numerical dispersion.

5 Studying the Thikhonov regularization with different constraints by the SVD and GSVD decompositions

In this section, at first, definitions of SVD and GSVD methods [19] are briefly reviewed. Thereafter, with these methods, effects of constraints Ω_1^2, Ω_2^2, and Ω_3^2 with and without a

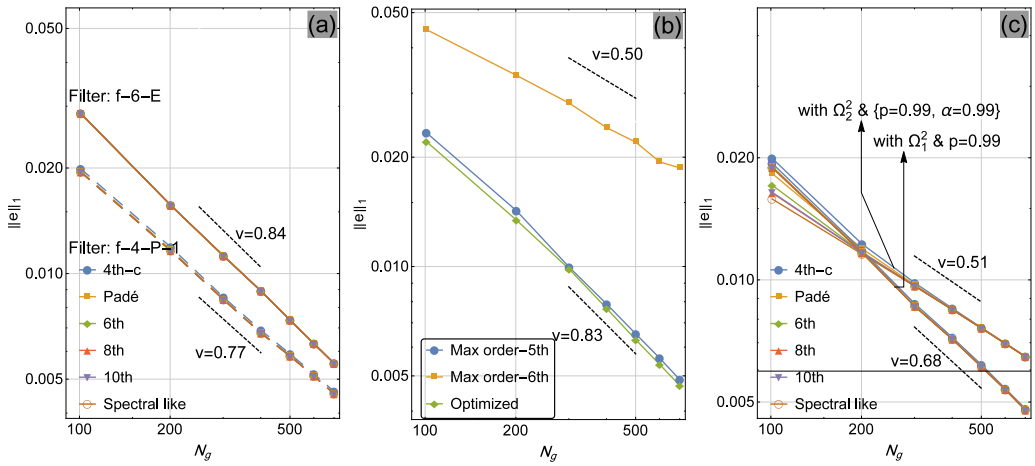

Figure 6: Convergence rates in the l_1 norm for different FD methods for discontinuous solutions.

model-solution ($\mathbf{f}_{model}$) will be studied.

The SVD decomposition The SVD decomposition of a rectangular matrix $\mathbf{A}\in\mathbb{R}^{m\times n}$ is: $\mathbf{A}=\mathbf{U}\mathbf{\Sigma}\mathbf{V}^T=\sum_{i=1}^{n}\mathbf{u}_i\sigma_i\mathbf{v}_i^T$. Matrices $\mathbf{U}=\{\mathbf{u}_1,\cdots,\mathbf{u}_n\}\in\mathbb{R}^{m\times n}$ and $\mathbf{V}=\{\mathbf{v}_1,\cdots,\mathbf{v}_n\}\in\mathbb{R}^{n\times n}$ are unitary matrices containing respectively the left singular($\mathbf{u}_i\in\mathbb{R}^m$) and right singular ($\mathbf{v}_i\in\mathbb{R}^n$) vectors. The matrix $\mathbf{\Sigma}=\text{diag}(\sigma_1,\cdots,\sigma_n)$ is diagonal and contains singular values σ_i, where $\sigma_i\geq\sigma_{i+1}$ & $\sigma_i\geq 0$.

The GSVD decomposition Let us assume: $\mathbf{A}\in\mathbb{R}^{m\times n}$ and $\mathbf{L}\in\mathbb{R}^{p\times n}$, where: $m\geq n\geq p$ and $\mathcal{N}(\mathbf{A})\cap\mathcal{N}(\mathbf{L})=\{\mathbf{0}\}$ (symbol $\mathcal{N}$ shows the null space). Then the GSVD of $(\mathbf{A},\mathbf{L})$ is [19]:

$$\mathbf{A}=\mathbf{U}\begin{pmatrix}\mathbf{\Sigma} & \mathbf{0}\\ \mathbf{0} & \mathbf{I}_{n-p}\end{pmatrix}\mathbf{X}^{-1},\qquad \mathbf{L}=\mathbf{V}(\mathbf{M},\mathbf{0})\mathbf{X}^{-1},\tag{5.1}$$

where: $\mathbf{U}\in\mathbb{R}^{m\times n}$; $\mathbf{V}\in\mathbb{R}^{p\times p}$; $\mathbf{X}\in\mathbb{R}^{n\times n}$. Matrices $\mathbf{U}$ and $\mathbf{V}$ have the unitary feature; and $\mathbf{X}$ is a non-singular matrix. Matrices $\mathbf{\Sigma}$ and $\mathbf{M}$ are non-negative diagonal matrices as: $\mathbf{\Sigma}=\text{diag}\{\sigma_1,\sigma_2,\cdots,\sigma_p\}$ and $\mathbf{M}=\text{diag}\{\mu_1,\mu_2,\cdots,\mu_p\}$. The singular values have following properties: 1) $1\geq\sigma_p\geq\sigma_{p-1}\geq\cdots\geq\sigma_1>0$; 2) $1\geq\mu_1\geq\mu_2\geq\cdots\geq\mu_p>0$; 3) $\sigma_i^2+\mu_i^2=1$. The *generalized singular values* γ_i of $(\mathbf{A},\mathbf{L})$ is then equal to: $\gamma_i=\sigma_i/\mu_i$.

5.1 The Tikhonov method without a model (extra information)

Regarding the linear system $\mathbf{Ax}=\mathbf{b}$, functional of the Tikhonov regularization with constraint operator $\mathbf{L}$ is : $Q=\|\mathbf{Ax}-\mathbf{b}\|_2^2+\lambda\|\mathbf{Lx}\|_2^2$. It is easy to show that, the minimizing solution of Q is: $\mathbf{x}_{min}=(\mathbf{A}^T.\mathbf{A}+\lambda\mathbf{L}^T.\mathbf{L})^{-1}(\mathbf{A}^T.\mathbf{b})$. By substituting the SVD/GSVD decom-

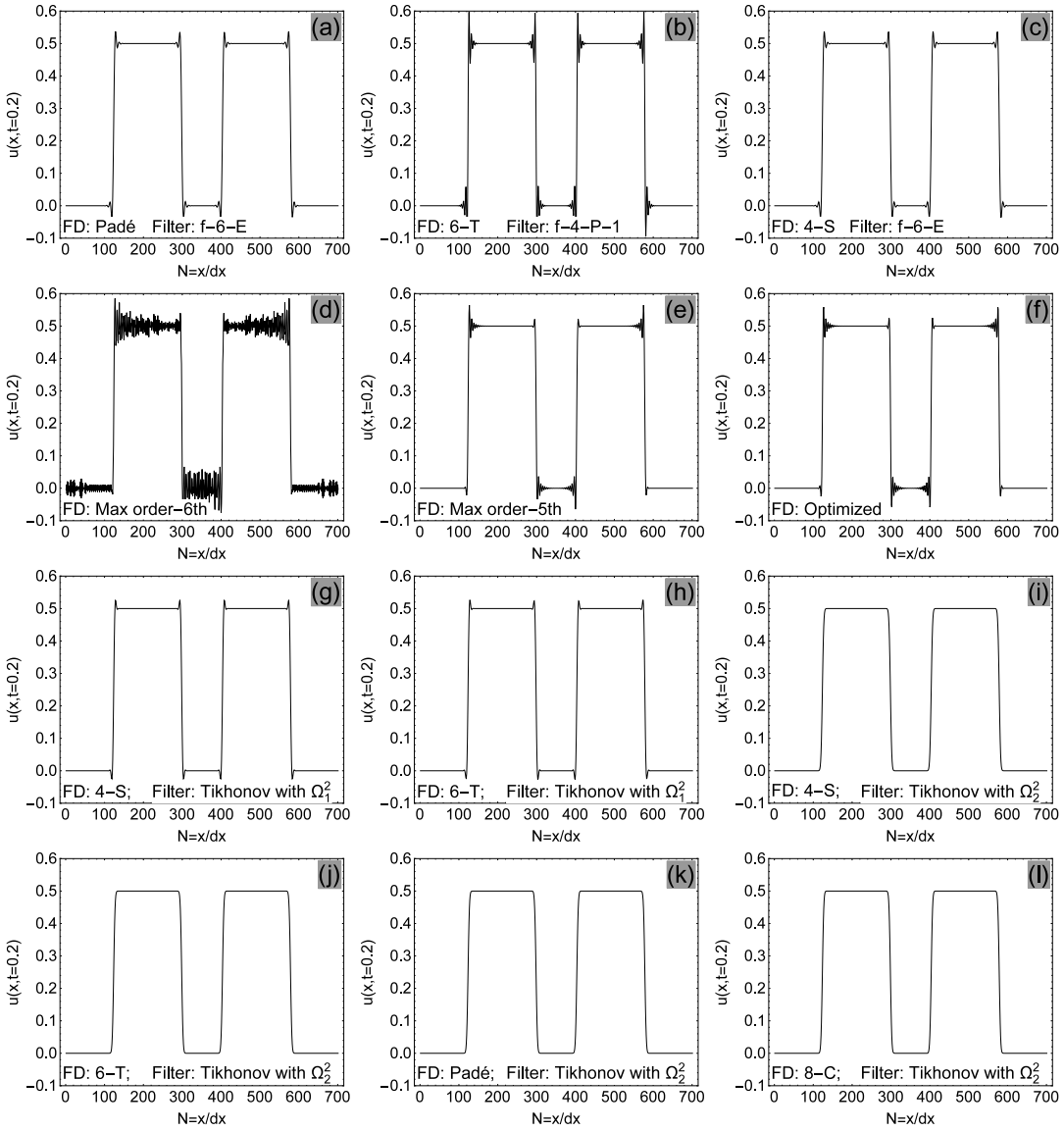

Figure 7: Discontinuous solutions $u(x,t=0.2)$ for different FD schemes and different filtering approaches.

posed forms of the operators, the $\mathbf{x}_{min}$ can be rewritten as [19]:

$$\mathbf{x}_{min}=\sum_{i=1}^{n}\frac{\mathbf{u}_i^T.\mathbf{b}}{\sigma_i}\mathbf{v}_i, \qquad \text{for} \qquad \lambda=0 \ \ (\text{without any regularization}),$$

$$\mathbf{x}_{min}=\sum_{i=1}^{n}F_i\frac{\mathbf{u}_i^T.\mathbf{b}}{\sigma_i}\mathbf{v}_i: \qquad F_i=\frac{\sigma_i^2}{\sigma_i^2+\lambda}, \qquad \text{for} \qquad \mathbf{L}=\mathbf{I},$$

$$\mathbf{x}_{min}=\sum_{i=1}^{p}F_i\frac{\mathbf{u}_i^T.\mathbf{b}}{\sigma_i}\mathbf{x}_i+\sum_{i=p+1}^{n}(\mathbf{v}_i^T.\mathbf{b})\mathbf{x}_i: \ F_i=\frac{\gamma_i^2}{\gamma_i^2+\lambda} \qquad \text{for} \qquad \mathbf{L}\neq\mathbf{I}. \tag{5.2}$$

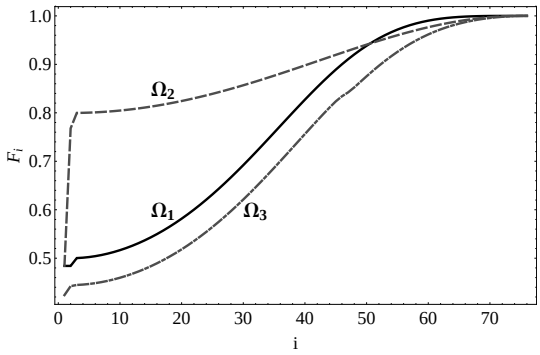

Figure 8: Filter coefficients for different constraints in the Tikhonov method, where $p=0.8$ & $\alpha=1$.

In the above equations, F_i acts as a filter; it damps effects of singular values with small values. For solutions obtained without regularization (i.e.: $\lambda=0$), the solution $\mathbf{x}_{min}$ would be sensitive for σ_i values of small (or nearly zero) values. They amplify corresponding $\mathbf{v}_i$ vector effects: the vectors with high fluctuations. Hence a proper inverse solution $\mathbf{x}_{min}$ is not obtainable.

In the following, performance of F_i values for the Tikhonov regularization method with different constraints will be studied. The constraints are: 1) $\Omega_1^2(x)=\int_{-\infty}^{+\infty}(f''(x))^2\mathrm{d}x$; 2) $\Omega_2^2(x)=\int_{-\infty}^{+\infty}(f''(x)+\alpha f'(x))^2\mathrm{d}x$; 3) $\Omega_3^2(x)=\int_{-\infty}^{+\infty}(f''(x)^2+\alpha^2 f'(x)^2)\mathrm{d}x$.

For numerical study, the Heaviside function, $H(x)$ is considered for spatial domain: $-1.5\leq x\leq 1.5$. The function is uniformly sampled at 76 points. In Fig. 8, F_i values are presented for these three constraints with parameter $p=0.8$ and $\alpha=1$. The figure offers that filters due to the constraint Ω_1^2 and Ω_3^2 have the same trend, but the latter leads to smaller filter coefficients. The constraint Ω_2^2 has a different trend and has larger filter values for small i values.

Regularized solutions according to Eq. (5.2) are presented in Fig. 9; it is clear that the Tikhonov method with Ω_2 constraint can effectively control the numerical dispersion.

The final stage for this problem is checking the discrete Picard condition; this condition states that to be sure that a regularization scheme works properly, corresponding $|\mathbf{u}_i.\mathbf{b}|$ values should on average decay toward zero faster than corresponding generalized singular values γ_i. This comparison is done in Fig. 10 for the three constraints. It is clear that results from constraints Ω_1 and Ω_2 satisfy completely the condition and the constraint Ω_3, on average meets the discrete Picard condition.

5.2 The Tikhonov method with a model (extra information)

If it is assumed that we have a model for a solution, like $(\mathbf{b}_{model})_{p\times 1}$, and $\mathbf{L}\neq\mathbf{I}$, then the corresponding functional is: $Q=\|\mathbf{A}\mathbf{x}-\mathbf{b}\|_2^2+\lambda\|\mathbf{L}(\mathbf{x}-\mathbf{b}_{model})\|_2^2$. It is straightforward to show that the solution is: $\mathbf{x}_{min}=(\mathbf{A}^T.\mathbf{A}+\lambda\mathbf{L}^T.\mathbf{L})^{-1}\{\mathbf{A}^T.\mathbf{b}+\lambda\mathbf{L}^T.\mathbf{L}.\mathbf{b}_{model}\}$. If we set $\mathbf{L}.\mathbf{b}_{model}=\mathbf{b}_{model}^L$ (this setting helps more clarifying behavior of regularized solutions) and using the

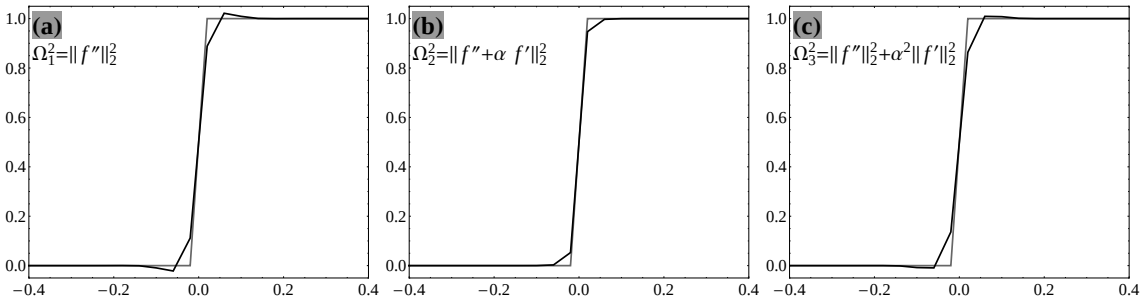

Figure 9: Regularized solutions with different constraints, where $p=0.8$ & $\alpha=1$.

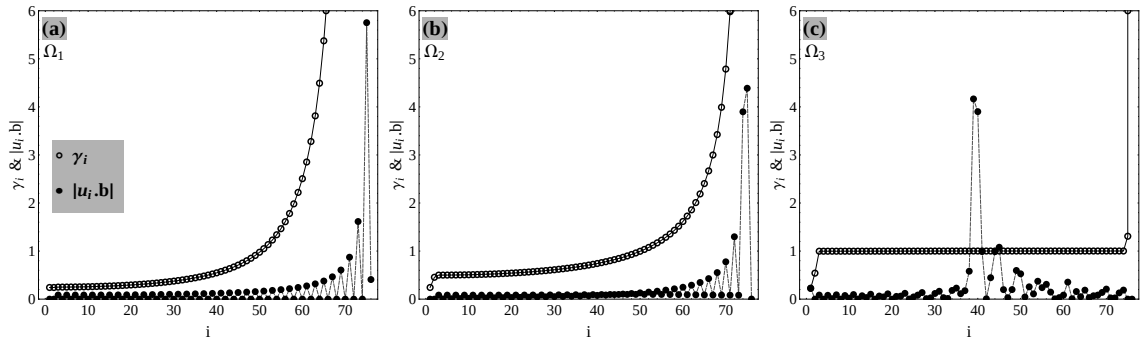

Figure 10: Control of the discrete Picard condition for regularized solutions with different constraints, where $p=0.8$ & $\alpha=1$.

GSVD, it is easy to show that the solution $\mathbf{x}_{min}$ can be written as:

$$\mathbf{x}_{min}=\left\{\sum_{i=1}^{p}F_i\frac{\mathbf{u}_i^T.\mathbf{b}}{\sigma_i}\mathbf{x}_i+\sum_{i=p+1}^{n}(\mathbf{v}_i^T.\mathbf{b})\mathbf{x}_i\right\}+\left\{\sum_{i=1}^{p}\alpha_i\frac{\mathbf{v}_i^T.\mathbf{b}_{model}^L}{\mu_i}\mathbf{x}_i\right\}, \tag{5.3}$$

where: $F_i=\frac{\gamma_i^2}{\gamma_i^2+\lambda}$ and $\alpha_i=\frac{\lambda}{\gamma_i^2+\lambda}$.

Depending on λ values, two extreme conditions can be happened: 1) if $\lambda\gg 0$, then $\alpha_i\to 1$; 2) if $\lambda\to 0$ then $\{F_i\to 1\ \&\ \alpha_i\to 0\}$. For the case (1), μ_i coefficients of small values cause oscillations in regularized solutions and in the case (2), filter coefficients F_i do not filter out oscillations. Hence, it is clear that why oscillation effects always remain in the regulated solutions. This effect will be amplified in discontinuous solutions (as numerically shown in numerical simulation of the 1D stress wave propagation problem, Section 3).

6 Implementation algorithms

In this section, implementation algorithms of Tikhonov-based regularization schemes will be presented.

Regarding sampled data $\{y_i\}$for $i\in\{1,2,\cdots,n\}$, the functional Q of the Tikhonov method is:

$$Q=\sum_{i=1}^{n}(y_i-f_i)^2+\lambda\times\Omega(f)_2^2. \tag{6.1}$$

In a more general form, in case of continuous functions $y:=y(x)$, the functional Q can be rewritten as:

$$Q=\int_{-\infty}^{+\infty}(y-f)^2\mathrm{d}x+\lambda\times\Omega(f)_2^2. \tag{6.2}$$

The solution f is the stationary point (extreme) of functional Q. For different $\Omega(f)$ definitions, corresponding implementation algorithms will be provided.

Using the finite difference approximation for discrete values $\{f(x_i):i=1,2,\cdots,n\}$, the order-$m$ derivative can be approximated as: $\mathbf{f}^{(m)}\approx\mathbf{D}^{(m)}.\mathbf{f}$. Derivative Matrices $\mathbf{D}^{(1)}$ and $\mathbf{D}^{(2)}$ can be approximated for uniform grids as:

$$\mathbf{D}^{(1)}=\frac{1}{\Delta x}\begin{pmatrix}-1&1&&\\-1&1&&\\&\ddots&\ddots&\\&&-1&1\end{pmatrix}_{n\times n},$$
$$\mathbf{D}^{(2)}=\frac{1}{\Delta x^2}\begin{pmatrix}1&-2&1&&\\1&-2&1&&\\&\ddots&\ddots&\ddots&\\&&1&-2&1\\&&1&-2&1\end{pmatrix}_{n\times n}, \tag{6.3}$$

where $\Delta x=x_{i+1}-x_i$ is the uniform sampling step in spatial domain. The $\mathbf{D}^{(1)}$ and $\mathbf{D}^{(2)}$ matrices, both have first-order spatial accuracy.

For numerically discretization of an integral (e.g., the integral in Eq. (6.2)), it can be approximated as:

$$\int_{x_1}^{x_n}|f(x)|^2\mathrm{d}x\approx\mathbf{f}^T.\mathbf{B}.\mathbf{f}, \tag{6.4}$$

where $\mathbf{B}$ denotes the integration rule matrix; for the midpoint integration rule, we have:

$$\int_{x_1}^{x_n}|f(x)|^2\mathrm{d}x\approx\frac{1}{2}(-x_1+x_2)f_1^2+\sum_{i=2}^{n-1}\left\{\frac{1}{2}(-x_{i-1}+x_{i+1})f_i^2\right\}+\frac{1}{2}(-x_{n-1}+x_n)f_n^2, \tag{6.5}$$

or

$$\int_{x_1}^{x_n}|f(x)|^2\mathrm{d}x\approx\frac{1}{2}f_1(-x_1+x_2)f_1+\sum_{i=2}^{n-1}\left\{\frac{1}{2}f_i(-x_{i-1}+x_{i+1})f_i\right\}+\frac{1}{2}f_n(-x_{n-1}+x_n)f_n. \tag{6.6}$$

So, the matric **B** can be obtained as:

$$\int_{x_1}^{x_n}|f(x)|^2\mathrm{d}x\approx\mathbf{f}^T.\left\{\frac{1}{2}\mathrm{diag}(-x_1+x_2,-x_1+x_3,\cdots,-x_{n-2}+x_n,-x_{n-1}+x_n)\right\}.\mathbf{f}$$
$$=\mathbf{f}^T.\mathbf{B}.\mathbf{f}, \tag{6.7}$$

where: $\mathrm{diag}\{a_1,\cdots,a_n\}$ shows a $n\times n$ diagonal matrix with diagonal elements a_i; the vector $\mathbf{f}$ denotes $\mathbf{f}=\{f_1,\cdots,f_n\}^T$.

Considering above-mentioned derivative and integral approximations, the minimizing solution, $\mathbf{f}_{min}$, for the Tikhonov regularization with different constraints will be presented in the following.

Tikhonov regularization with constraint: $\Omega_2^2=\int_{-\infty}^{+\infty}(f''(x)+\alpha f'(x))^2\mathrm{d}x$**.** Firstly, the functional $Q(\mathbf{f})$ is rewritten as:

$$Q(\mathbf{f})=\int(y-f)^2\mathrm{d}x+\lambda\times\left\{\int\left(f''^2+\alpha^2f'^2+2\alpha f'f''\right)\mathrm{d}x\right\}, \tag{6.8}$$

The discretized form of the functional Q is:

$$Q(\mathbf{f})=(\mathbf{y}-\mathbf{f})^T.\mathbf{B}.(\mathbf{y}-\mathbf{f})+\lambda$$
$$\times\left\{\left(\mathbf{D}^{(2)}\mathbf{f}\right)^T.\mathbf{B}.\left(\mathbf{D}^{(2)}\mathbf{f}\right)+\alpha^2\left(\mathbf{D}^{(1)}\mathbf{f}\right)^T.\mathbf{B}.\left(\mathbf{D}^{(1)}\mathbf{f}\right)+2\alpha\left(\mathbf{D}^{(1)}\mathbf{f}\right)^T.\mathbf{B}.\left(\mathbf{D}^{(2)}\mathbf{f}\right)\right\}, \tag{6.9}$$

To find minimizing solution, the functional Q is minimized with respect to $\mathbf{f}$ as:

$$\frac{\partial Q(\mathbf{f})}{\partial\mathbf{f}}=-2\mathbf{B}.(\mathbf{y}-\mathbf{f})+\lambda$$
$$\times\left\{2\left(\mathbf{D}^{(2)}\right)^T.\mathbf{B}.\left(\mathbf{D}^{(2)}.\mathbf{f}\right)+2\alpha^2\left(\mathbf{D}^{(1)}\right)^T.\mathbf{B}.\left(\mathbf{D}^{(1)}.\mathbf{f}\right)+2\alpha\left(\mathbf{D}^{(2)}\right)^T.\mathbf{B}.\left(\mathbf{D}^{(1)}.\mathbf{f}\right)\right.$$
$$\left.+2\alpha\left(\mathbf{D}^{(1)}\right)^T.\mathbf{B}.\left(\mathbf{D}^{(2)}.\mathbf{f}\right)\right\}=0. \tag{6.10}$$

Hence, the minimizing solution $\mathbf{f}_{min}$ is:

$$\mathbf{f}_{min}=\left\{\mathbf{B}+\lambda\left(\mathbf{D}^{(2)}\right)^T.\mathbf{B}.\mathbf{D}^{(2)}+\lambda\alpha^2\left(\mathbf{D}^{(1)}\right)^T.\mathbf{B}.\mathbf{D}^{(1)}\right.$$
$$\left.+\lambda\alpha\left(\mathbf{D}^{(2)}\right)^T.\mathbf{B}.\mathbf{D}^{(1)}+\lambda\alpha\left(\mathbf{D}^{(1)}\right)^T.\mathbf{B}.\mathbf{D}^{(2)}\right\}^{-1}.(\mathbf{B}.\mathbf{y}). \tag{6.11}$$

Tikhonov regularization with constraint: $\Omega_3^2=\int_{-\infty}^{+\infty}(f''(x)^2+\alpha^2 f'(x)^2)\mathrm{d}x$**.** In this case, by following the previous procedure for finding $\mathbf{f}_{min}$ for Ω_2^2, it is easy to show that the solution is the same as Eq. (6.11), but this time without first and second derivative interaction terms; i.e.:

$$\mathbf{f}_{min}=\left\{\mathbf{B}+\lambda\left(\mathbf{D}^{(2)}\right)^T.\mathbf{B}.\mathbf{D}^{(2)}+\lambda\alpha^2\left(\mathbf{D}^{(1)}\right)^T.\mathbf{B}.\mathbf{D}^{(1)}\right\}^{-1}.(\mathbf{B}.\mathbf{y}). \tag{6.12}$$

Some remarks

1. Minimizing solution $f_{min}(x)$ for the commonly used Tikhonov regularization method with constraint $\Omega_1^2=\int_{-\infty}^{+\infty}f''(x)^2\mathrm{d}x$ can simply be obtainable by setting $\alpha=0$ in Eq. (6.11) or (6.12) (without any tension effect).
2. For weighted residual norm, i.e.: $\|W_i(y_i-f_i)\|_2^2$, with weights W_i, variable smoothing ($\lambda=\lambda(x)$) and variable tension ($\alpha=\alpha(x)$) parameters, it is easy to show that Eq. (6.11) can be written as:

$$\begin{aligned}\mathbf{f}_{min}=\Big\{&\mathbf{W}.\mathbf{B}+\boldsymbol{\lambda}.\left(\mathbf{D}^{(2)}\right)^T.\mathbf{B}.\mathbf{D}^{(2)}+\left(\boldsymbol{\lambda}.\boldsymbol{\alpha}.\boldsymbol{\alpha}^T\right).\left(\mathbf{D}^{(1)}\right)^T.\mathbf{B}.\mathbf{D}^{(1)}\\&+(\boldsymbol{\lambda}.\boldsymbol{\alpha}).\left(\mathbf{D}^{(2)}\right)^T.\mathbf{B}.\mathbf{D}^{(1)}+(\boldsymbol{\lambda}.\boldsymbol{\alpha}).\left(\mathbf{D}^{(1)}\right)^T.\mathbf{B}.\mathbf{D}^{(2)}\Big\}^{-1}.(\mathbf{W}.\mathbf{B}.\mathbf{y}),\end{aligned} \tag{6.13}$$

   where: $\mathbf{W}=\mathrm{diag}\{W_1,W_2,\cdots,W_n\}$; $\boldsymbol{\lambda}=\mathrm{diag}\{\lambda_1,\lambda_2,\cdots,\lambda_n\}$; $\boldsymbol{\alpha}=\mathrm{diag}\{\alpha_1,\alpha_2,\cdots,\alpha_n\}$. Corresponding algorithm for constraint Ω_3^2 can easily be obtained by canceling first and second derivative interaction effects in Eq. (6.13). For the common Tikhonov method (with Ω_1^2 constraint) by setting the tension term to zero, corresponding algorithm is obtainable.
3. For the model-based Tikhonov regularization with general constraint $\Omega_2^2=\int_{-\infty}^{+\infty}(f''(x)+\alpha f'(x))^2\mathrm{d}x$, it is easy to show that the corresponding numerical algorithm is:

$$\mathbf{f}_{min}=\{\mathbf{B}+\lambda\boldsymbol{\Gamma}\}^{-1}\{\mathbf{B}.\mathbf{y}+\lambda\boldsymbol{\Gamma}.\mathbf{f}_{model}\}, \tag{6.14}$$

   where:

$$\boldsymbol{\Gamma}=\left\{\left(\mathbf{D}^{(2)}\right)^T.\mathbf{B}.\mathbf{D}^{(2)}+\alpha^2\left(\mathbf{D}^{(1)}\right)^T.\mathbf{B}.\mathbf{D}^{(1)}+\alpha\left(\mathbf{D}^{(2)}\right)^T.\mathbf{B}.\mathbf{D}^{(1)}+\alpha\left(\mathbf{D}^{(1)}\right)^T.\mathbf{B}.\mathbf{D}^{(2)}\right\}. \tag{6.15}$$

4. According to the aforementioned numerical implementation algorithms, since all matrices are sparse and banded, the algorithms are fast and cost-effective.
5. It should be mentioned that regularized results can have grid dependency feature; this means to have the same regularized results on finer or coarser grids, different regularization parameters should be used (i.e., p and α). To prevent this grid dependency, here, sampled data are remapped in a way that the new sampling step becomes unit, i.e.: $\Delta x=1$.

7 Errors and convergence rates

7.1 Convergence rate for the Tikhonov method with different constraints

The Tikhonov method with constraints Ω_1^2 and Ω_3^2 are special cases of (m,s)-splines (for case $s=0$, this family becomes D^m-splines [2]) and (m,l,s)-splines (also known as $L^{m,l,s}$-splines), respectively [54]. The (m,s)-splines are a special case of (m,l,s)-splines for $l=0$ [54]. To be exact, $(2,0)$-splines and $(1,1,0)$-splines are solutions of the 1-D Tikhonov method with constraints Ω_1^2 and Ω_3^2, respectively. For these two general spline families, error bounds and convergence rates are studied even in presence of noise [2, 44, 54].

The aim of this sub-section is to show roughly that the Tikhonov method with constraint Ω_2^2 is also bounded and has the convergence property.

Functional of Tikhonov methods with constraints Ω_2^2 and Ω_3^2 are respectively denoted by Q_2 and Q_3; on the finite domain $x\in[x_1,x_{N_g}]$, it is easy to show that Q_2 relates to Q_3 as:

$$Q_2=Q_3+2\alpha\lambda\int_{x_1}^{x_{N_g}} f''f'dx, \tag{7.1}$$

where N_g denotes number of grid points, $f':=df/dx$ and $f'':=d^2f/dx^2$. Minimizing solution of both Q_2 and Q_3 are L-splines; these splines can be written as bellow on the spatial domain $x_i\le x\le x_{i+1}=x_i+\Delta x$, [30, 43]:

$$f_i(x)=a_i+b_i(x-x_i)+c_ie^{\alpha(x-x_i)}+d_ie^{-\alpha(x-x_i)}, \tag{7.2}$$

where, Δx is an uniform sampling step, and coefficients $\{a_i,b_i,c_i,d_i\}$ are unknown, real and bounded values. Using Eq. (7.2), functional $\int f''f'dx$ on $x_i\le x\le x_i+\Delta x$ leads to:

$$\begin{aligned}\gamma_i:=&\int_{x_i}^{x_i+\Delta x} f''f'dx\\ =&\frac{1}{2}\alpha e^{-2\alpha\Delta x}\left(-1+e^{\alpha\Delta x}\right)\left(d_i+c_ie^{\alpha\Delta x}\right)\left(2b_ie^{\alpha\Delta x}+\left(1+e^{\alpha\Delta x}\right)\left(-d_i+c_ie^{\alpha\Delta x}\right)\alpha\right).\end{aligned} \tag{7.3}$$

Using the Taylor series, γ_i can be expanded as:

$$\gamma_i=\left[b_ic_i\alpha^2+b_id_i\alpha^2+c_i^2\alpha^3-d_i^2\alpha^3\right]\Delta x+\left[\frac{1}{2}b_ic_i\alpha^3-\frac{1}{2}b_id_i\alpha^3+c_i^2\alpha^4+d_i^2\alpha^4\right]\Delta x^2+O\left[\Delta x^3\right], \tag{7.4}$$

or:

$$\gamma_i=\left[b_i(c_i+d_i)+\left(c_i^2-d_i^2\right)\alpha\right]\alpha^2\Delta x+O[\Delta x^2]. \tag{7.5}$$

Since coefficients $\{a_i,b_i,c_i,d_i\}$ are real and bounded values, so there exists a real and positive value such C_i where: $\gamma_i\le C_i\alpha^2\Delta x$. By integration of γ_i on the domain $x\in[x_1,x_{N_g}]$, the following inequality can be obtained between Q_2 and Q_3:

$$Q_3-2\alpha^3\lambda\Delta x\left(\sum_{i=1}^{N_g-1}C_i\right)\le Q_2\le Q_3+2\alpha^3\lambda\Delta x\left(\sum_{i=1}^{N_g-1}C_i\right). \tag{7.6}$$

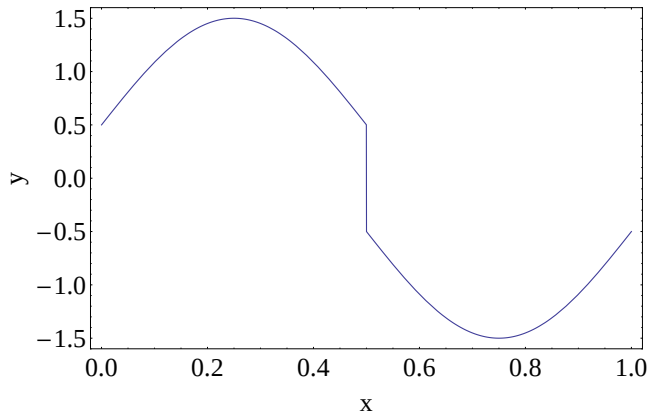

Figure 11: The test function $y(x)$.

It is clear that, $\lim_{\Delta x\to 0} Q_2 = Q_3$. Hence, Q_2 is bounded and has the convergence property; its convergence rate also approaches to functional Q_3 as sampling step approaching zero.

7.2 A benchmark problem

As studied before, the constraint Ω_2^2 in the Tikhonov method can control the numerical dispersion. In this section, the *error in estimation* and *convergence rate* will numerically be studied by a benchmark problem. The problem has both smooth and discontinuous features. By this example, both the ***numerical dispersion*** and ***Runge*** phenomena are investigated. The function is:

$$y(x) = \frac{1}{2} + \sin(2\pi x) - H(x-0.5), \tag{7.7}$$

where $H(x)$ denotes the Heaviside function; the function $y(x)$ is illustrated in Fig. 11.

In Fig. 12, the regulated results obtained by constraints Ω_1^2 (the common Tikhonov method) and Ω_2^2 are compared with each other. Considered parameters are: 1) for the case Ω_1^2: $p=0.9$; 2) for the case Ω_2^2: $p=0.9$ & $\alpha=1$. From this figure, it is clear that using the constraint Ω_2^2 leads to: 1) developing of more localized errors (of large magnitudes) around discontinuous solutions; 2) rising of larger errors in smooth regions; 3) controlling of the numerical dispersion more effectively; 4) increasing of the Runge phenomenon around boundaries. Fig. 13 presents convergence rates of different solutions for the two constraints. It is obvious that: 1) convergence rates are near to each other and for all of them, corresponding rates are near to 0.6; 2) with the same p values, the Ω_2^2 constraint leads to less numerical errors in L_1 and L_2 senses (even though the errors resulted from the Ω_2^2 are more than those of Ω_1^2 in smooth regions). The difference of two estimated errors, resulted from two different constraints Ω_1^2 and Ω_2^2, increases considerably as p values approach to one.

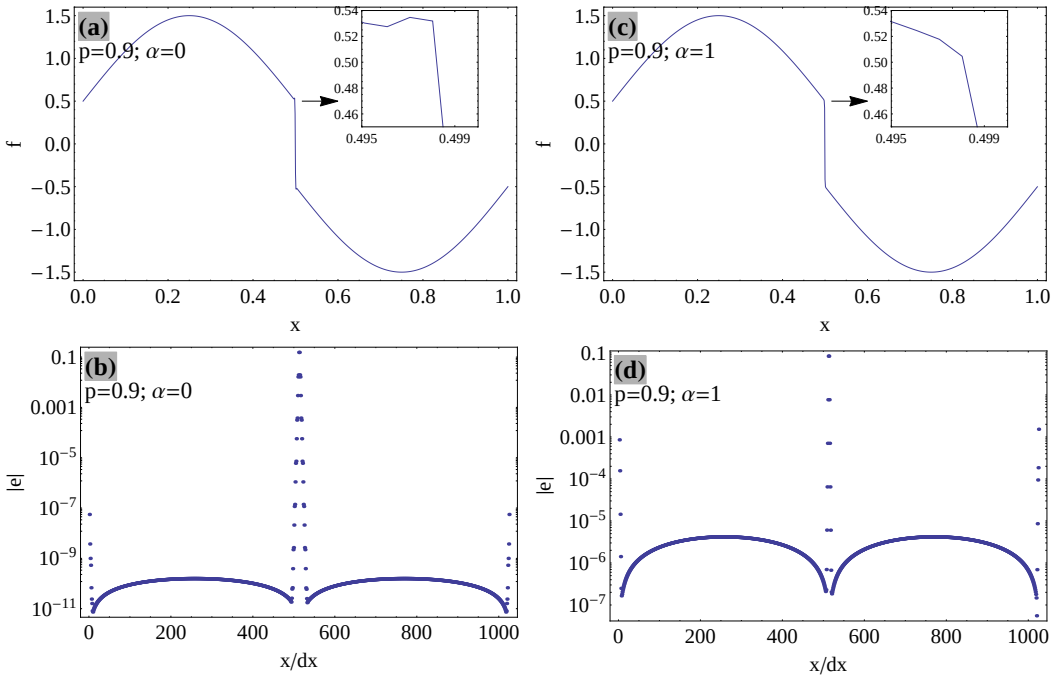

Figure 12: Error in estimations, the numerical dispersion and Runge phenomena resulted from the Tikhonov method with different constraints; (a) & (b) regularization with constraint Ω_1^2; (c) & (d) regularization with constraint Ω_2^2;

As mentioned before, the constraint Ω_2^2 leads to both: 1) larger the Runge phenomenon (around boundaries); 2) larger estimated errors in smooth regions. To cure these drawbacks, one effective way is to use variable tension (α) values. The values can be close to zero in smooth regions; it can locally be increased around high gradient or discontinuous zones. Regarding the test function $y(x)$ (Eq. (7.7)), a Gaussian function for $\alpha(x)$ is assumed: it is centered around the discontinuity (with spatial location $x=0.5$). The estimated solution, corresponding estimation errors and convergence rates are presented in Fig. 14 for $p=0.9$. Figs. 14(a), (b) and (c) present the estimated solution, estimation error, and convergence rate, respectively. The results offer that the non-uniform estimation both improves accuracy of estimations in smooth areas and decreases the Runge phenomenon around boundaries. In this case, the numerical dispersion is successfully controlled, as well.

8 Conservation in Tikhonov-based smoothing

For sampled data $\{y_i\}$ with Gaussian noise, the Tikhonov-based regularization finds smoothed data $\{f_i\}$ in such a way that: $y_i = f_i + \varepsilon_i$; where: the set $\{\varepsilon_i\}$ denotes the noise with zero mean, i.e.: $\sum_i \varepsilon_i = 0$ [57]. In this case, filtered data remain conservative,

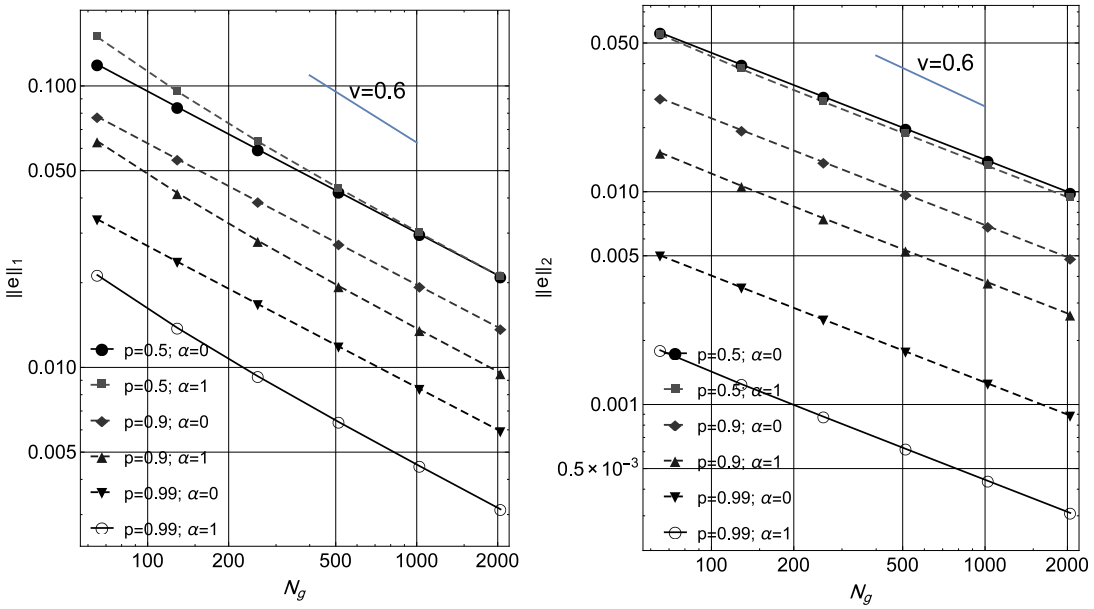

Figure 13: Convergence rates for Tikhonov regularization in L_1 and L_2 norms with the constraints Ω_1^2 and Ω_2^2 for different p and α values.

since: $\sum_i y_i = \sum_i f_i$. In numerical simulations, however, such assumption for noise type is not true and thereby smoothed data do not remain conservative.

Conservative smoothing, however, can be obtained by imposing an extra constraint in the Tikhonov method, as:

$$Q=\sum_{i=1}^{n}(y_i-f_i)^2+\lambda\,\Omega^2(f),$$
$$\text{subjected to:}\quad \frac{1}{n}(\mathbf{I}.\mathbf{y})=\frac{1}{n}(\mathbf{I}.\mathbf{f}),\quad \left(\text{i.e.:}\sum_i y_i=\sum_i f_i\right) \tag{8.1}$$

where: $\mathbf{I}_{1\times n}$ denotes a single row matrix with unit elements, as: $\mathbf{I}_{1\times n}=[1,\cdots,1]_{1\times n}$; vectors $\mathbf{f}$ and $\mathbf{y}$ are: $\mathbf{f}=[f_1,\cdots,f_n]^T$ and $\mathbf{y}=[y_1,\cdots,y_n]^T$. Using the Lagrange multiplier method, the modified functional, Q_L becomes:

$$Q_L=\sum_{i=1}^{n}(y_i-f_i)^2+\lambda\,\Omega^2(f)+\lambda^L\left\{\frac{1}{n}(\mathbf{I}.(\mathbf{f}-\mathbf{y}))^T\right\}, \tag{8.2}$$

where λ^L is the Lagrange coefficient. For case $\Omega^2(f)=\Omega_1^2(f)=\int(f''(x))^2dx$, extremes of

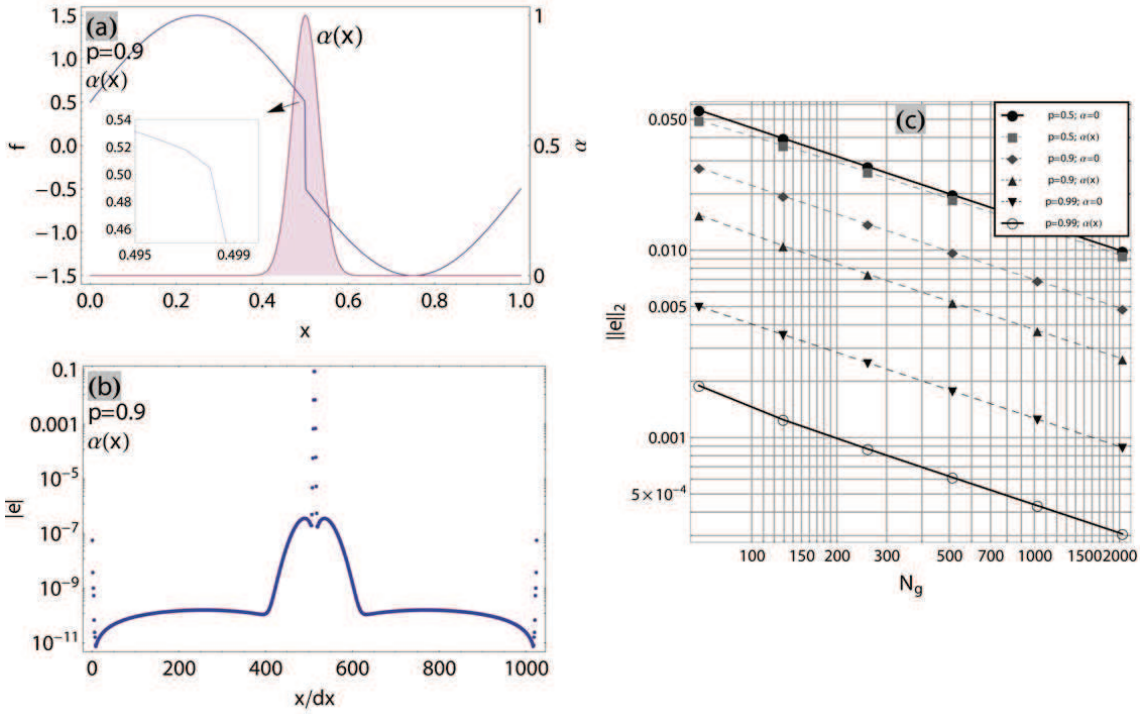

Figure 14: Variable α parameter in Tikhonov-based regularization with the constraint Ω_2^2; a) regularized results (f) and $\alpha(x)$; b) estimation errors; c) convergence rates.

the functional Q_L with respect to $\mathbf{f}$ and λ^L are:

$$\frac{\partial Q_L}{\partial \mathbf{f}} = \mathbf{0} \Rightarrow \underbrace{2\left[\mathbf{B}+\lambda\left\{\left(\mathbf{D}^{(2)}\right)^T.\mathbf{B}.\mathbf{D}^{(2)}\right\}\right]}_{\Gamma}.\mathbf{f}+\frac{\lambda^L}{n}\mathbf{I}^T = 2\mathbf{B}.\mathbf{y},$$
$$\frac{\partial Q_L}{\partial \lambda^L} = 0 \Rightarrow \frac{1}{n}(\mathbf{I}.\mathbf{y}) = \frac{1}{n}(\mathbf{I}.\mathbf{f}). \tag{8.3}$$

These equations lead to the following linear system:

$$\begin{bmatrix} \Gamma & \frac{\mathbf{I}^T}{n} \\ \frac{\mathbf{I}}{n} & 0 \end{bmatrix} \begin{bmatrix} \mathbf{f} \\ \lambda^L \end{bmatrix} = \begin{bmatrix} 2\mathbf{B}.\mathbf{y} \\ (\mathbf{I}.\mathbf{y})/n \end{bmatrix}. \tag{8.4}$$

Obtaining of such linear systems for other $\Omega^2(f)$ definitions are straightforward.

Example 8.1. Linear data $\{\{(x_i,y_i)\}=\{(i,i)\};\quad i=1,\cdots,7\}$ is perturbed as:

$$\{(x_i,y_i)\}=\{\{1,1\},\{2,2.01\},\{3,2.97\},\{4,3.99\},\{5,5.03\},\{6,6\},\{7,7\}\}.$$

Using the conservative Tikhonov regularization with parameter $p=0.9$, smoothed data will be:

$$\{f_i\}=\{1.005100307,2.000351,2.9790275,3.99291,5.0189070,6.005833,6.9978714\}.$$

In this case, we have:$\sum_i y_i-\sum_i f_i=2.07\times10^{-12}$ ($\sum_i y_i=28$ & $\sum_i f_i=28$).

For the common Tikhonov regularization (without the constraint of the conservative smoothing), the smoothed result is:

$$\{f_i\}=\{1.0054894578,2.979230914,3.993112981,5.01911043,6.006076,6.9982605\};$$

where: $\sum_i f_i=28.0019$. It is clear the smoothing is not conservative.

The constraint of conservative smoothing can also be imposed by the *penalty* method in the functional Q, as:

$$Q_P=\sum_{i=1}^{n}(y_i-f_i)^2+\lambda\ \Omega^2(f)+C^P\left\{\left[\frac{1}{n}(\mathbf{I}.(\mathbf{f}-\mathbf{y}))^T\right].\left[\frac{1}{n}(\mathbf{I}.(\mathbf{f}-\mathbf{y}))\right]\right\}, \tag{8.5}$$

where C^P is a predefined penalty coefficient.

9 Global and local smoothing

The common Tikhonov method leads to global smoothing. Two approaches can be followed to have local smoothing (regularization): i) local regularization (with consistency with surrounding data); ii) global regularization with variable weights and/or smoothing parameters. Below the first approach will be discussed.

9.1 Local regularization

The main idea is to smooth only some local zones of data. At boundary points of the local zones, continuity of both smoothed data and corresponding derivatives (up to some order) should be preserved with surrounding information. To have such local Tikhonov regularization, the concept of smoothing with constraints can be used for local zones of data. These extra constraints guarantee continuity at boundary points. The functional Q subjected to some new extra constraints can be expressed as:

$$\begin{aligned} &Q=\sum_i(y_i-f_i)^2+\lambda\Omega^2(f),\\ &\text{subjected to: } \left\{\overline{\mathbf{A}}_j.\mathbf{f}^{(j)}=\mathbf{y}_0{}^{(j)}:\quad j\in\{0,1,\cdots,m\}\ \&\ f\in C^m\right\}, \end{aligned} \tag{9.1}$$

where: $\mathbf{f}^{(0)}:=\mathbf{f}$; $\mathbf{y}_0{}^{(0)}=\mathbf{y}_0$; $\mathbf{f}^{(j)}:=d^j\mathbf{f}/dx^j$ & $\mathbf{y}_0{}^{(j)}:=d^j\mathbf{y}_0/dx^j$, for $j\geq1$; $f_i:=f(x_i)$; $\{\mathbf{f}=\{f_i\}:$ $i\in\{1,\cdots,n\}\}$ denotes the smooth function needed to be estimated at distinct n spatial

points; $\mathbf{y}_0{}^{(j)}=\{(y_0^{(j)})_k\}$ is a vector of data values needed to be interpolated at some predefined points (like boundary points). For a predefined point x_k then it is needed to have: $\{f^{(j)}(x_k)=y_0{}^{(j)}(x_k):\ j\in\{0,1,\cdots,m\}\}$; Matrix $\overline{\mathbf{A}}_j$ denotes a connection matrix of size $n\times r$, where n and r are vector lengths of $\mathbf{f}$ and $\mathbf{y}_0$, respectively. At the spatial location x_k, for l^{th} element of $\mathbf{y}_0{}^{(j)}$ (i.e.: $(\mathbf{y}_0{}^{(j)}(x_k))_{l,1}$), element $(\overline{\mathbf{A}}_j)_{l,k}$ is equal to one and remaining elements of the l^{th} row are zero.

Using the Lagrange multiplier to impose extra constraints, the new functional Q_L is:

$$Q_L=\sum_i (y_i-f_i)^2+\lambda\,\Omega^2(f)+\sum_{j=0}^{m}\boldsymbol{\lambda}_j^L\left(\overline{\mathbf{A}}_j.\mathbf{f}^{(j)}-\mathbf{y}_0{}^{(j)}\right)^T, \tag{9.2}$$

where $\boldsymbol{\lambda}_j^L$ denotes a Lagrange multiplier vector.

By finding extreme values of Q_L with respect to $\mathbf{f}$ and vectors $\{\boldsymbol{\lambda}_j^L\}$, one can find both $\mathbf{f}$ and $\{\boldsymbol{\lambda}_j^L\}$. Let assume $f(x)\in C^2$, and $\Omega^2(f)=\Omega_1^2(f)=\int (f''(x))^2dx$; then it is easy to obtain a discretized form of Q_L, as:

$$\begin{aligned}Q_L=&(\mathbf{y}-\mathbf{f})^T.\mathbf{B}.(\mathbf{y}-\mathbf{f})+\lambda\left(\mathbf{D}^{(2)}.\mathbf{f}\right)^T.\mathbf{B}.\left(\mathbf{D}^{(2)}.\mathbf{f}\right)+\boldsymbol{\lambda}_0^L(\overline{\mathbf{A}}_0.\mathbf{f}-\mathbf{y}_0)^T\\&+\boldsymbol{\lambda}_1^L\left(\overline{\mathbf{A}}_1.\left(\mathbf{D}^{(1)}.\mathbf{f}\right)-\mathbf{y}_0{}'\right)^T+\boldsymbol{\lambda}_2^L\left(\overline{\mathbf{A}}_2.\left(\mathbf{D}^{(2)}.\mathbf{f}\right)-\mathbf{y}_0{}''\right)^T,\end{aligned} \tag{9.3}$$

where $\mathbf{f}^{(1)}$ and $\mathbf{f}^{(2)}$ are respectively approximated as, $\mathbf{D}^{(1)}.\mathbf{f}$ and $\mathbf{D}^{(2)}.\mathbf{f}$.

Extreme values of Q_L can be obtained, as:

$$\begin{aligned}&\frac{\partial Q_L}{\partial\mathbf{f}}=\mathbf{0}\Rightarrow\underbrace{2\left[\mathbf{B}+\lambda\left\{\left(\mathbf{D}^{(2)}\right)^T.\mathbf{B}.\mathbf{D}^{(2)}\right\}\right]}_{\boldsymbol{\Gamma}}.\mathbf{f}+\boldsymbol{\lambda}_0^L.\overline{\mathbf{A}}_0{}^T+\boldsymbol{\lambda}_1^L.\left(\overline{\mathbf{A}}_1.\mathbf{D}^{(1)}\right)^T+\boldsymbol{\lambda}_2^L.\left(\overline{\mathbf{A}}_2.\mathbf{D}^{(2)}\right)^T\\&\qquad=2\mathbf{B}.\mathbf{y},\\&\frac{\partial Q_L}{\partial\boldsymbol{\lambda}_0^L}=\mathbf{0}\Rightarrow\overline{\mathbf{A}}_0.\,\mathbf{f}=\mathbf{y}_0,\\&\frac{\partial Q_L}{\partial\boldsymbol{\lambda}_1^L}=\mathbf{0}\Rightarrow\left(\overline{\mathbf{A}}_1.\mathbf{D}^{(1)}\right).\,\mathbf{f}=\mathbf{y}_0{}',\\&\frac{\partial Q_L}{\partial\boldsymbol{\lambda}_2^L}=\mathbf{0}\Rightarrow\left(\overline{\mathbf{A}}_2.\mathbf{D}^{(2)}\right).\,\mathbf{f}=\mathbf{y}_0{}''.\end{aligned} \tag{9.4}$$

These equations can be represented in a matrix form, as:

$$\begin{pmatrix}\boldsymbol{\Gamma}&\overline{\mathbf{A}}_0^T&\left(\overline{\mathbf{A}}_1.\mathbf{D}^{(1)}\right)^T&\left(\overline{\mathbf{A}}_2.\mathbf{D}^{(2)}\right)^T\\\overline{\mathbf{A}}_0&\mathbf{0}&\mathbf{0}&\mathbf{0}\\\left(\overline{\mathbf{A}}_1.\mathbf{D}^{(1)}\right)&\mathbf{0}&\mathbf{0}&\mathbf{0}\\\left(\overline{\mathbf{A}}_2.\mathbf{D}^{(2)}\right)&\mathbf{0}&\mathbf{0}&\mathbf{0}\end{pmatrix}.\begin{bmatrix}\mathbf{f}\\\boldsymbol{\lambda}_0^L\\\boldsymbol{\lambda}_1^L\\\boldsymbol{\lambda}_2^L\end{bmatrix}=\begin{bmatrix}2\mathbf{B}.\mathbf{y}\\\mathbf{y}_0\\\mathbf{y}_0{}'\\\mathbf{y}_0{}''\end{bmatrix}. \tag{9.5}$$

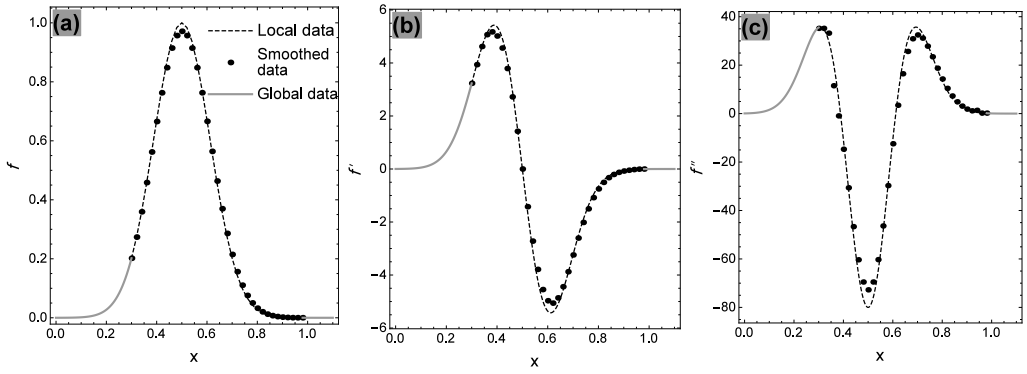

Figure 15: Local smoothing with C^2 continuity with surrounding data; value of smoothing parameter is $p=0.7$.

The above left-hand side matrix can be ill-posed, in general. For such cases, the extra constraints can be imposed by the penalty method. In this case, the functional Q can be modified as:

$$Q_P=\sum_i (y_i-f_i)^2+\lambda\ \Omega^2(f)+\sum_{j=0}^{m} C_j^P\left(\overline{\mathbf{A}}_j.\mathbf{f}^{(j)}-\mathbf{y}_0{}^{(j)}\right)^T\left(\overline{\mathbf{A}}_j.\mathbf{f}^{(j)}-\mathbf{y}_0{}^{(j)}\right), \tag{9.6}$$

where C_j^P denotes predefined penalty coefficients.

For an example, an exponential function is assumed, as: $y(x)=\mathrm{Exp}(-40(x-0.5)^2)$. The aim is the local smoothing on spatial range $0.30\le x\le 0.98$ in such a way that the smoothed data have C^2 continuity with surrounding data. Edge constraints (on y, $y^{'}$ and $y^{''}$) are only imposed for two boundary end points $x=0.30$ and $x=0.98$ (more boundary points can be assumed for each edge). Smoothed results are presented in Fig. 15, where the smoothing parameter is $p=0.7$. In this figure, discrete values of $\mathbf{f}^{'}$ and $\mathbf{f}^{''}$ are computed with the same operators used in the regularization procedure, i.e.: $\mathbf{f}^{'}=\mathbf{D}^{(1)}.\mathbf{f}$ and $\mathbf{f}^{''}=\mathbf{D}^{(2)}.\mathbf{f}$. It is clear that the local smoothed data and corresponding derivatives have consistency with neighbor data.

10 Tikhonov regularization and correspondence with filtering

It is mentioned that the regularization effect is similar to a low-pass filtering [57]. Constraints of the Tikhonov method measure high-frequency components of data; these components are then enforced to approach zero. This filtering feature will be studied in more detail in this section.

Regarding functional $Q=\int F(x,y,y^{'},y^{''})dx$, where $y:=y(x)$, $y^{'}:=dy/dx$ and $y^{''}:=d^2y/dx^2$, it is easy to show that corresponding Euler-Lagrange differential equation is: $F_y-\frac{d}{dx}(F_{y'})+\frac{d^2}{dx^2}(F_{y''})=0$, where: $F_y:=dF/dy$, $F_{y'}:=dF/dy^{'}$ and $F_{y''}:=dF/dy^{''}$.

For the Tikhonov regularization with constraint $\Omega_2^2(x)=\int (f''+\alpha f')^2 dx$, the function F is: $F(x,f,f',f'')=(y-f)^2+\lambda(f''+\alpha f')^2$. It is straightforward to show that equivalent Euler-Lagrange equation for constant λ and α is:

$$-(y-f)-\lambda\alpha^2 f''+\lambda f^{(iv)}=0. \tag{10.1}$$

Rewriting this equation in the Fourier space, we have:

$$\mathcal{F}(f)-\mathcal{F}(y)-\lambda\alpha^2(i\omega)^2\mathcal{F}(f)+\lambda(i\omega)^4\mathcal{F}(f)=0, \tag{10.2}$$

or,

$$\mathcal{F}(f)=\frac{1}{1+\lambda\alpha^2\omega^2+\lambda\omega^4}\mathcal{F}(y), \tag{10.3}$$

where: $\mathcal{F}(f)$ denotes the Fourier transform of the function $f(x)$ belonging to the Hilbert space L_2 (i.e.: $\int f(x)^2 dx<\infty$); $i^2=-1$; and $\omega\in[0,\pi]$. So using the constraint $\Omega_2^2(x)$ leads to the filter function $H_2(\omega)$ as:

$$H_2(\omega)=1/\left(1+\lambda\alpha^2\omega^2+\lambda\omega^4\right). \tag{10.4}$$

For constraints $\Omega_1^2(x)$ and $\Omega_3^2(x)$, it is easy to show that corresponding filter functions are:

$$\begin{aligned} H_1(\omega)&=1/\left(1+\lambda\omega^4\right),\\ H_3(\omega)&=1/\left(1+\lambda\alpha\omega^2+\lambda\omega^4\right). \end{aligned} \tag{10.5}$$

It is clear that: 1) $H_j(0)=1$ and $H_j(\pi)=0$ for $j\in\{1,2,3\}$; 2) thereby, functions $\{H_j(\omega)\}$ act as low-pass filters. In fact, they are a type of Butterworth low pass filters [57].

11 Solution algorithm for stress wave equations

The main idea is to use the regularization stage as a post-processing step in the commonly used finite-difference (or collocation) method with higher-order accuracy. For this reason, consider the solution of a second order hyperbolic system to be $\mathbf{f}(t)$. At time step t_n, the solution procedure can be summarized as the following steps:

1. Approximate spatial derivatives with finite difference discretizations; this can be done by the generalized Padé approximations, compact differencing equations (see Section 4) [35,69] or the fast and iterative algorithm proposed by Fornberg [14]. In this work, explicit fourth order spatial accuracy is used for derivative estimations (to have a higher-order solver),

2. Discretize PDEs in the spatial domain and solve resulted semi-discrete systems, i.e., discrete in space and continuous in time. A standard time-stepping method like the Runge-Kutta method of 4^{th} order (see Appendix A) or the explicit six-stage method [69] can be used to solve the resulted ODEs at time $t=t_n$ to obtain solution at the next time step $t=t_{n+1}$,
3. Denoise spurious oscillations (this step can be done directly on non-uniform grid points, as well); for this purpose the Tikhonov method with constraint Ω_2^2 is recommended. Either variable or constant p or α values can be considered. In this work, constant values are used. The recommended values for p and α are: $0.9\leq p\leq 0.99$, and $\alpha\approx 1$. For the Tikhonov method other extra conditions can also be considerable; such as: conservative (Section 8) or local (Section 9) smoothing.
4. Go back to step 1,

In practice, to have a cost-effective computation, the solution is not denoised at each time step. This can be done after some time steps (depending on the wave velocity), for example following ten time steps.

12 Numerical examples

In this section, one 1D and several 2D examples are presented to show effectiveness of the proposed approach. The 2D examples are: 1) a membrane subjected to an imposed initial discontinuous deformation (to simulate propagating discontinuous fronts); 2) an infinite-periodic domain containing sharp and localized variation of physical property (a narrow fluid-filled crack with finite dimension); 3) wave propagation in a medium with several fluid-filled cavities with stochastic locations (to have stochastic-like simulations) [29,64].

In simulations, for Tikhonov methods it is assumed: 1) they are not enhanced to be conservative; 2) the global smoothing approach is used.

Example 12.1. In this example, the wave propagation in a 1D linear bar with the box-shaped initial imposed deformation is re-simulated (see Section 3) with other commonly-used approaches. They are basically developed to remedy discontinuity effects in elasto-dynamic problems. The methods are:

1. The finite element method with linear spatial shape functions using numerically dissipative time integration scheme (α-NDTI) [20]. The assumed parameters are: $\gamma=0.6$; $\beta=0.25(0.5+\gamma)^2$; $\alpha=-0.0683$; $dt=0.003$; number of elements is $N_e=256$.
2. Common Taylor-Galerkin method (TG-C) (second order) and higher order one (TG-HO) (third order) [65]; for the TG-C case, assumed parameters are: $\gamma=0.5$ and $\alpha=0.5$; $dt=0.002$; $N_e=256$. For the TG-HO method, two set of parameters are considered as: i) for TG-HO-1: $\gamma=0.5$; $\alpha=0.5$; $N_e=256$; $dt=0.002$; ii) for TG-HO-2: $\gamma=0.5$; $\alpha=1.5$; $N_e=256$; $dt=0.002$.

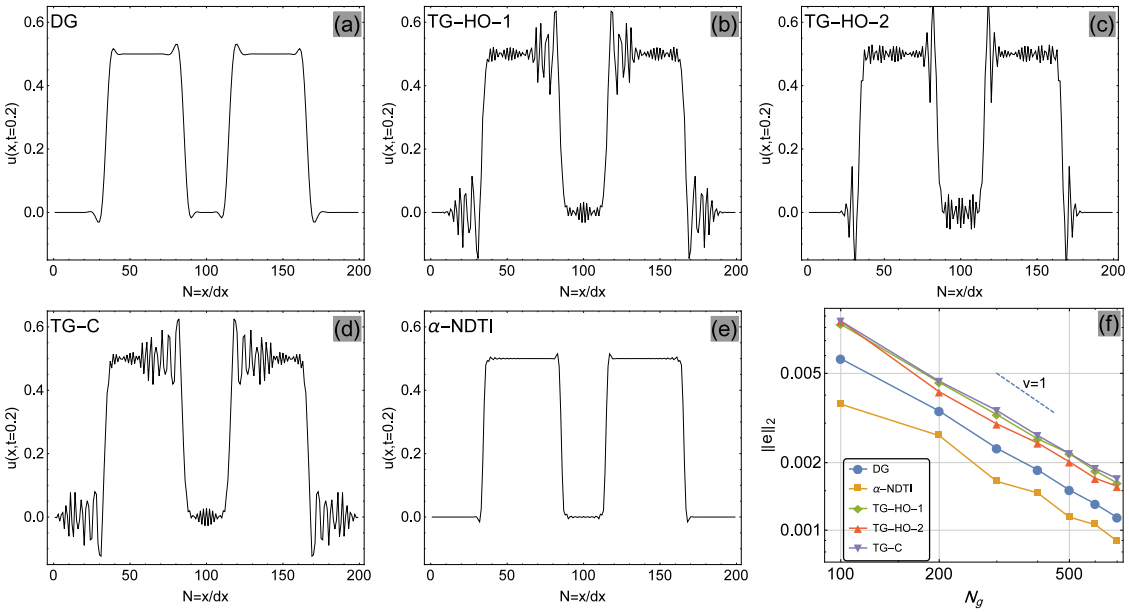

Figure 16: Numerical results for wave propagation in a bar due to the box-shaped imposed initial condition at $t=0.2$.

3. Discontinuous time Galerkin method (DTG) [38] (piece-wise linear approximations in the time and linear approximations in the space). The considered parameters are: $dt=0.01$ and $N_e=256$.

In each scheme, the considered parameters are the suggested values in the corresponding references, to have a good estimation of the exact solution. In appendix A, above-mentioned methods are briefly reviewed. For numerical simulations, properties of the bar are: $E=1$ (module of elasticity), $A=0.01$ (cross section area), and $\rho=1$ (density of the bar). The results are presented in Fig. 16. Although these methods lead to stable solutions, they can not effectively control the numerical dispersion.

As mentioned in the Introduction section, the idea of high-resolution schemes is recently extended to second order hyperbolic systems [3]. Bellow the aim is to compare such results with those of our proposed method. For this reason, this example is resolved on spatial domain $x\in[-1,1]$ with new initial conditions: $u_0(x)=$ Unitbox $(2x)$ and $v_0(x)=0$. For the Tikhonov method it is assumed: 1) smoothing is done at each time step; 2) The functional Ω_2^2 is used as the constraint; 3) smoothing parameters are: $p=0.99$ & $\alpha=1$.

Numerical results are presented in Fig. 17 at $t=0.2$; symbols $P-4$, $UW2$, $UW4$, and $HR2$ denote the 4^{th} order Padé, second order upwind, fourth order upwind and second-order high resolution approximations, respectively. For details of $UW2$, $UW4$, and $HR2$ methods, please see [3]. The results offer that: 1) smoothed $P-4$ method (using the Tikhonov smoothing method) prevents forming of spurious oscillations in both u and

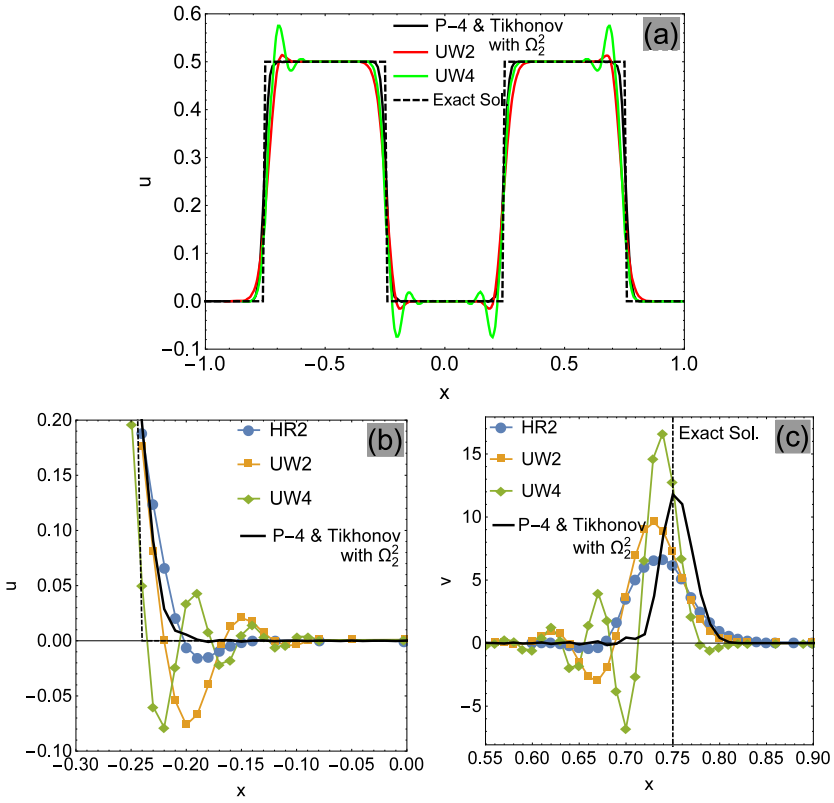

Figure 17: Direct simulation of the second order scalar wave propagation problem at $t=0.2$; symbols $P-4$, $UW2$, $UW4$ and $HR2$ denote the 4^{th} order Padé, second order upwind, fourth order upwind and second-order high resolution approximations, respectively. The results of $UW2$, $UW4$ and $HR2$ are from [3].

v solutions; 2) numerical dissipation of smoothed $P-4$ is less than those of $HR2$ and coincides with those of $UW2$ (Fig. 17(b)); 3) numerical dispersion in smoothed $P-4$ is the least one (Fig. 17(a,c)). The results of $UW2$, $UW4$, and $HR2$ are from [3].

Example 12.2. Consider vibration of a rectangular membrane with four fixed sides subjected to an initial imposed displacement; the governing equations are:

$$\begin{aligned} PDE&: \; c^2\left(\partial^2u/\partial x^2+\partial^2u/\partial z^2\right)=\partial^2u/\partial t^2; \;\; \Omega\in[0,1]\times[0,1],\\ ICs&: \; u(x,y,t=0)=U(x,y) \;\; \& \;\; \partial u/\partial t(x,y,t=0)=0,\\ BCs&: \; u(0,y,t)=u(1,y,t)=u(x,0,t)=u(x,1,t)=0. \end{aligned} \tag{12.1}$$

The initial condition has discontinuities; it is: $U(x,y)=H((\frac{x-0.5}{0.2})^2+(\frac{y-0.5}{0.2})^2)$ (where H denotes the Heaviside function). The finite difference scheme is used for spatial discretization; the second derivative is approximated with the fourth-order explicit central scheme; number of grid points is: $(2^8+1)\times(2^8+1)$. The time-integration is done by the Runge-Kutta scheme of 4^{th} order (see Appendix A). For the post-processing stage, the

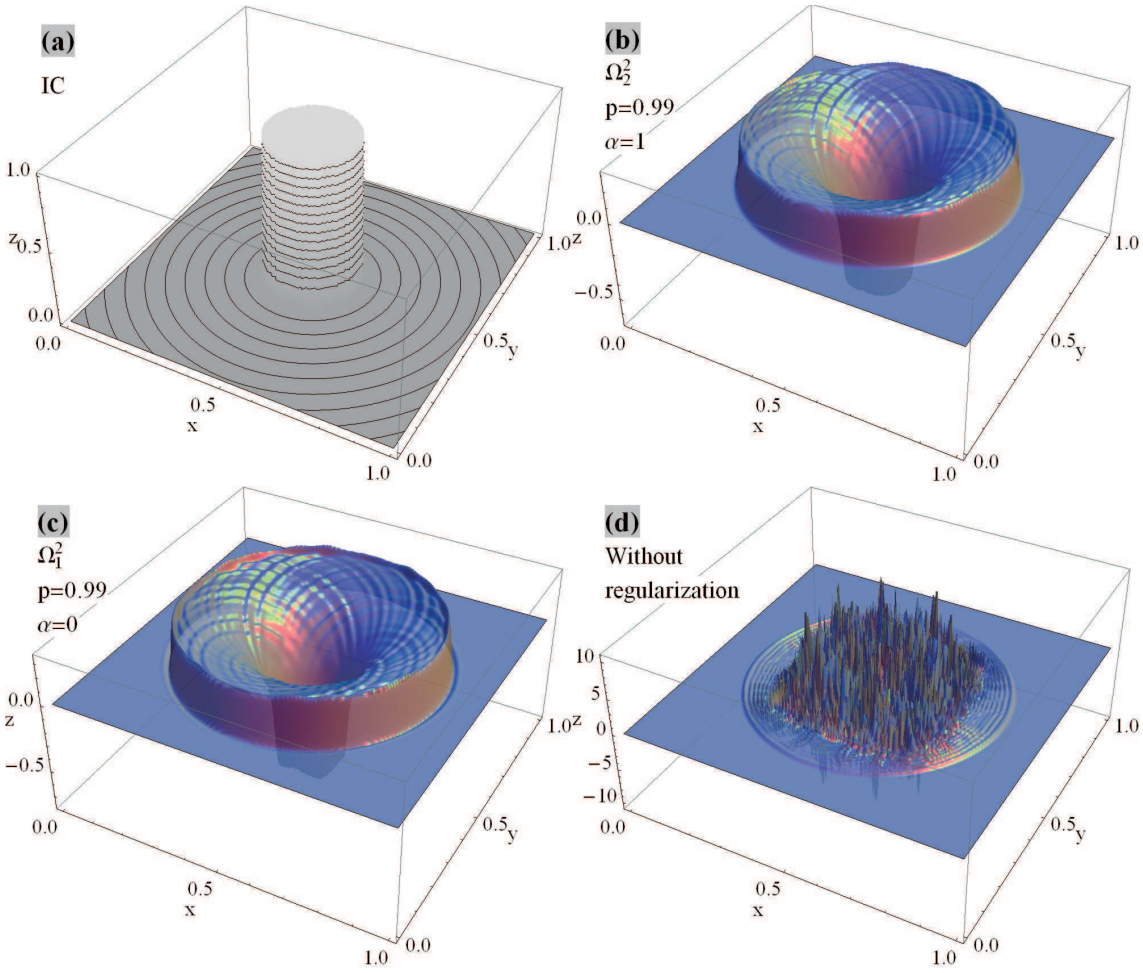

Figure 18: Numerical results with different assumptions of regularization constraints at $t=0.24$; a)the IC condition ($U(x,y)$); b) the solution based on using the constraint Ω_2^2; c) the solution based on using the constraint Ω_1^2; d) the solution without any regularization.

Tikhonov method with three different constraints are considered: 1) Ω_1^2 with the parameter $p=0.99$; 2) the constraint Ω_2^2 with parameters $p=0.99$ & $\alpha=1$; 3) $p=1$, i.e.: without considering any regularization. Other parameters are assumed to be: $c=1$ (wave velocity); $dt=0.0015$ (the time integration step). The denoising (regularization) procedure is repeated after each five time steps. The IC ($U(x,y)$) and numerical results are presented in Fig. 18 at $t=0.24$. According to the results, it is clear that: 1) without regularization, the solution becomes unstable; 2) small amount of the regularization leads to stable solutions; 3) results obtained by Ω_2^2 constraint can control more effectively spurious oscillations around propagating discontinuous fronts.

The numerical result obtained by the post-processing stage with constraint Ω_2^2 and

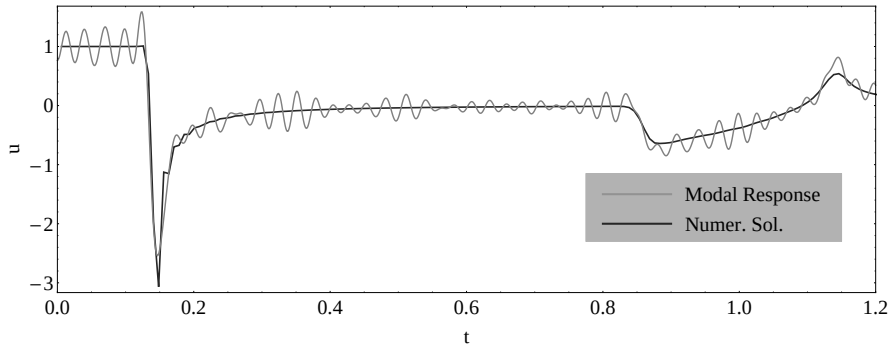

Figure 19: Comparison of the numerical method having the post-processing stage with constraint Ω_2^2, and the modal analysis based solution (with 60×60 first modes) at spatial position $(x,y)=(0.5,0.5)$.

the solution obtained from the modal analysis will also be compared. For the square membrane with dimensions $(x,y)\in[a\times b]$, and with four fixed boundaries, the mode shapes are:

$$M_{n,m}(x,y)=\sin\left(\frac{m\pi x}{a}\right)\times\sin\left(\frac{n\pi y}{b}\right), \tag{12.2}$$

The results are compared in Fig. 19 at spatial location $(x,y)=(0.5,0.5)$ for time duration $t\in[0,1.2]$. For the modal analysis, it is assumed: $(n,m)=(60,60)$ (i.e., 60×60 first modes are considered). Due to discontinuities, the numerical dispersion exists in the modal analysis. Therefor, a stable and oscillation free numerical result can be obtained by considering the post-processing stage (the constraint is: Ω_2^2).

Example 12.3. In this example, the stress wave propagation problem is studied in a medium including high and abrupt variations in its physical parameters. In such systems, numerical methods which can not handle (semi) discontinuous solutions (caused by the material variation) have stability and accuracy problems around contact zones (e.g., the fluid-solid contact zone). Due to this material variation, speeds of elastic waves are largely different around the contact zone. The incident waves, P or S, can be reflected from interface in the form of P and S waves. The incident P wave is reflected as P (denotes by PPr) and S (shown by PSr) waves; for the incident SV wave the reflected P and S waves are shown by SPr and SSr, respectively. If the second material is water, since only P waves can be transmitted to the fluid layer, the transmitted P wave due to incident P and S waves are denoted by PPt and SPt, respectively. Another phenomenon due to existence of a sharp corner is the diffraction. The P wave is diffracted from crack edges into the solid medium as diffracted P (PPd) and diffracted S (PSd) waves.

It is assumed that the medium has infinite-periodic boundaries, and it contains a narrow fluid-filled crack of finite length. Due to this crack, each P or S (SV) incident waves are reflected and transmitted. Also due to edge of the crack, the diffraction phenomenon will be happened.

The schematic shape of the medium along with the description of the crack configu-

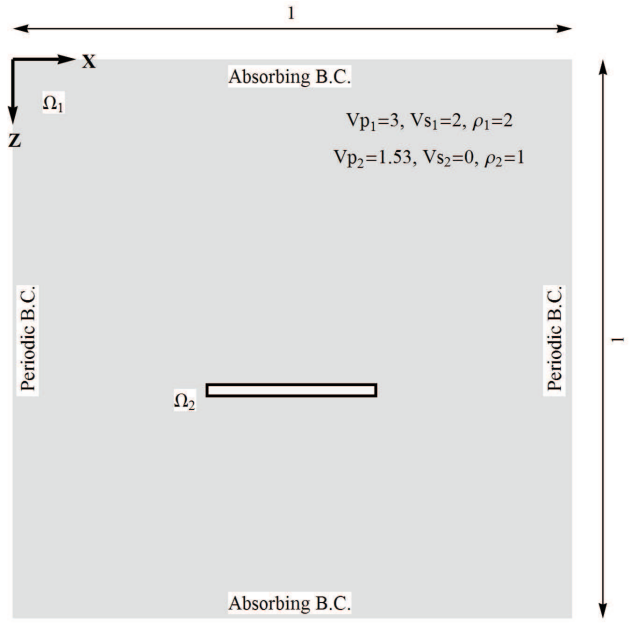

Figure 20: Schematic shape of an infinite-periodic medium including a fluid-filled narrow crack.

ration is illustrated in Fig. 20. There, position of periodic and absorbing boundary conditions are also illustrated.

Here, to consider infinite boundaries the absorbing boundary concept is used. This boundary is explicitly considered in the governing P-SV equations, as:

$$\begin{aligned}&\{(\lambda+2\mu)u_{x,xx}+\mu u_{x,zz}\}+\{(\lambda+\mu)u_{z,xz}\}=\rho\{u_{x,tt}+Q(x,z)u_{x,t}\},\\&\{(\lambda+2\mu)u_{z,zz}+\mu u_{z,xx}\}+\{(\lambda+\mu)u_{x,xz}\}=\rho\{u_{z,tt}+Q(x,z)u_{z,t}\}.\end{aligned}\tag{12.3}$$

The absorbing boundaries are commonly used for simulation of infinite boundaries. In this system, absorbing boundary condition is considered explicitly; or equivalently the wave equations are modified by damping term $Q(x,z)$. This acts as an attenuation factor. This factor is nearly zero in the computation domain and increases gradually when approaches to the artificial boundaries. This causes incoming waves towards these kind of boundaries to diminish gradually [55]. In general, there is not any absorbing boundary that could absorb all of the incoming energies, so, some small long-period reflections always remain. In this problem, the attenuation function is:

$$Q(x,z)=a_z\Big(Exp(b_z.z^2)+Exp(b_z.(1-z)^2)\Big),$$

where $a_z=120$ and $b_z=-100$.

In the numerical simulation, it is assumed that: 1) the post-processing stage is done by the Tikhonov method with constraint Ω_2^2; 2) the incident wave is a plane P wave,

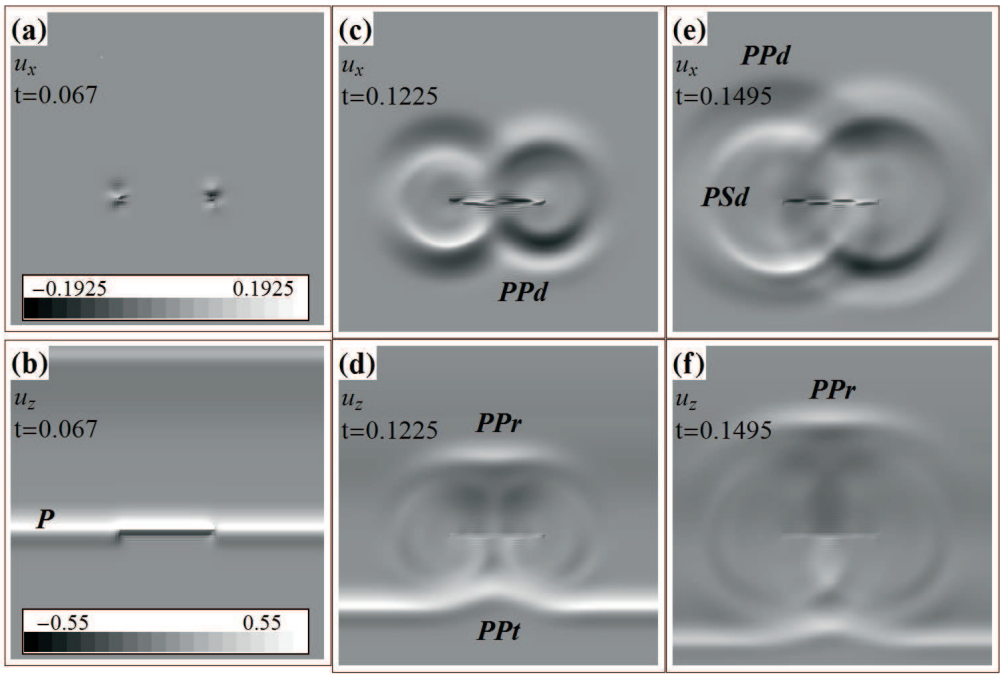

Figure 21: Snapshots of solutions u_x and u_z.

produced by an initial imposed deformation with equation: $u_z(x,z,t=0)=\text{Exp}(-700(z-0.25)^2)$; 3) the regularization is performed after each five time steps with parameters $p=0.97$ and $\alpha=1$; 4) time step is: $dt=0.001$; 5) number of grid points in each direction is: 2^8+1; 5) time-integration is done by the Runge-Kutta 4^{th} order method.

The snapshots of u_x and u_z are illustrated in Fig. 21. There, the reflected, transmitted and diffracted waves are shown. The zoomed-in solution u_z at incident time, $t=0.067$ is illustrated in Fig. 22; it is clear that formation of spurious oscillations are prevented due to discontinuous solutions formed around contact zone.

Example 12.4. Our concern in this example is controlling of artificial dispersion developing in stochastic like solutions. So, a wave propagation problem in a stochastic medium will be studied. In such systems, propagating fronts can not develop due to the diffraction phenomenon. The challenging problem is developing of dominate non-physical dispersive waves.

One practical approach for stochastic media simulation is to consider several stochastic fluid-filled small cavities in homogeneous media [29, 64]. The considered medium is illustrated in Fig. 23, where the black disks show the cavities. It is assumed that: 1) the medium has infinite-periodic boundary conditions; 2) a plane P wave propagates in the z direction.

In the numerical simulations, we have: 1) spatial discretization is done with the explicit central finite difference method of fourth order accuracy; 2) the time integration

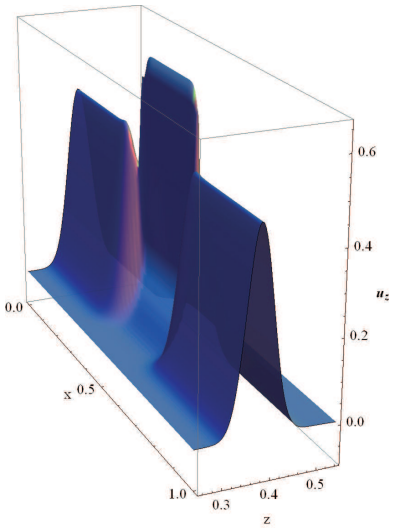

Figure 22: Snapshot of solutions u_z at $t=0.067$.

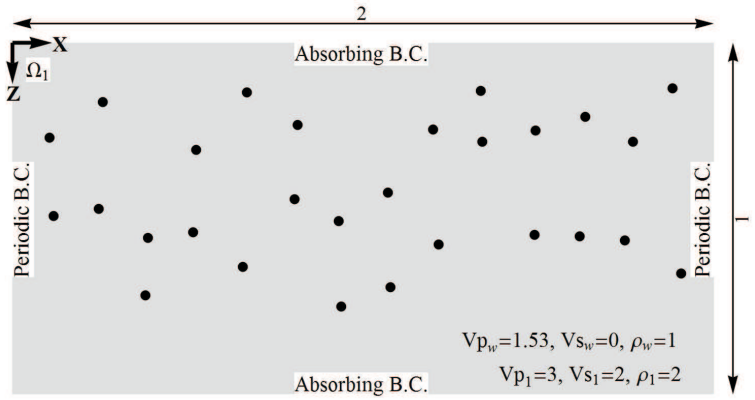

Figure 23: A homogeneous medium with stochastic fluid-filled small cavities.

method is the Runge-Kutta scheme of fourth order with time step $dt=0.001$; 3) post-processing stage is performed using the Tikhonov method with constraint Ω_2^2 and parameters $p=0.99$ and $\alpha=1$; and 4) the regularization repeats after each five time steps; 4) number of grid points is: $(2^9+1,2^8+1)$.

Snapshots of results for u_x and u_z are presented at Fig. 24 for different times. According to the u_x solutions, it is clear that the diffracted waves propagate and propagating fronts can not be formed in the domain due to stochastic nature of solutions.

Fig. 25 illustrates an investigation on the regularization effects. It compares two solutions of u_x with and without the regularization-stage (with the constraint Ω_2^2) at $t=0.0805$. It is shown that even marginal regularization can prevent occurrence of the artificial dispersion (commonly occurred in stochastic-like numerical solutions).

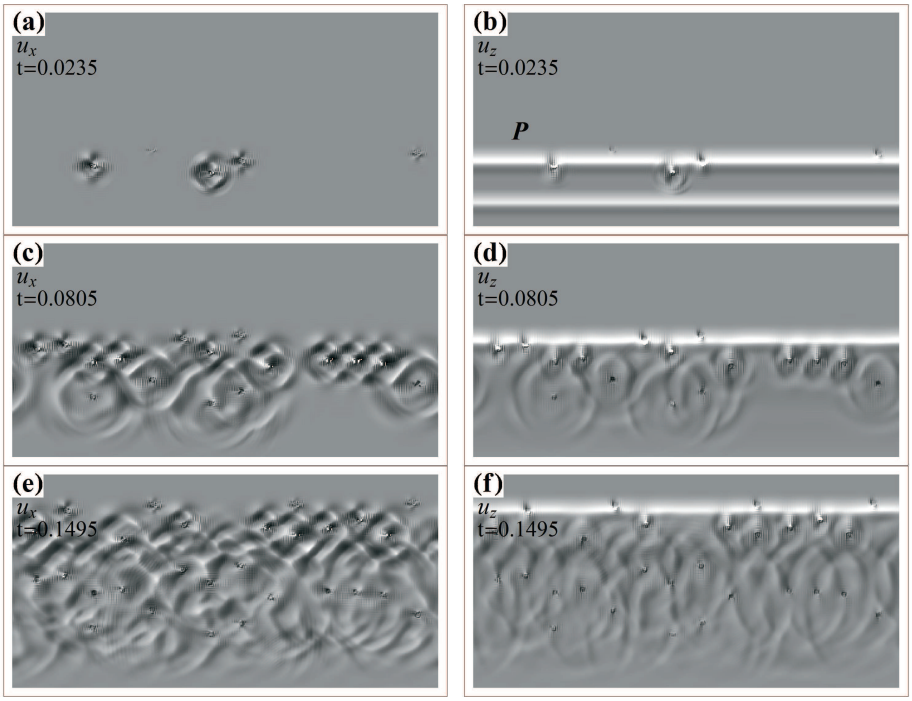

Figure 24: Formation of stochastic-like solutions u_x and u_z from the fluid-filled cavities due to diffraction of the incident plane P wave.

13 Conclusion

We have presented an approach including a post-processing stage to control the numerical dispersion around discontinuities for numerical simulation of the mechanical wave propagation problems (known as the second order hyperbolic PDEs). Several compact high-order finite-difference methods are successfully integrated with the Tikhonov method as a post-processor. This is done to control spurious oscillations formed around discontinuities due to the numerical dispersion. For this controlling, the crucial point is a proper choosing of a constraint for Tikhonov-based regularization. Different types of regularization with different constraints are studied. And finally a proper constrained with some possible extensions is advised.

Regarding Tikhonov method, two general approaches are studied: regularization with and without a model. A model contains extra almost local information (such as discontinuity locations) to improve regulated results. However, it is shown (by numerical studies and GSVD decomposition method), the model-based results are sensitive to the model; if the model is exact, the regulated solution can properly handle discontinuity effects, otherwise results are sensitive and the numerical dispersion affects them. It is shown that the constraint resulted from proper combination of smoothness and the tension concept can properly control the numerical dispersion around discontinuities. This

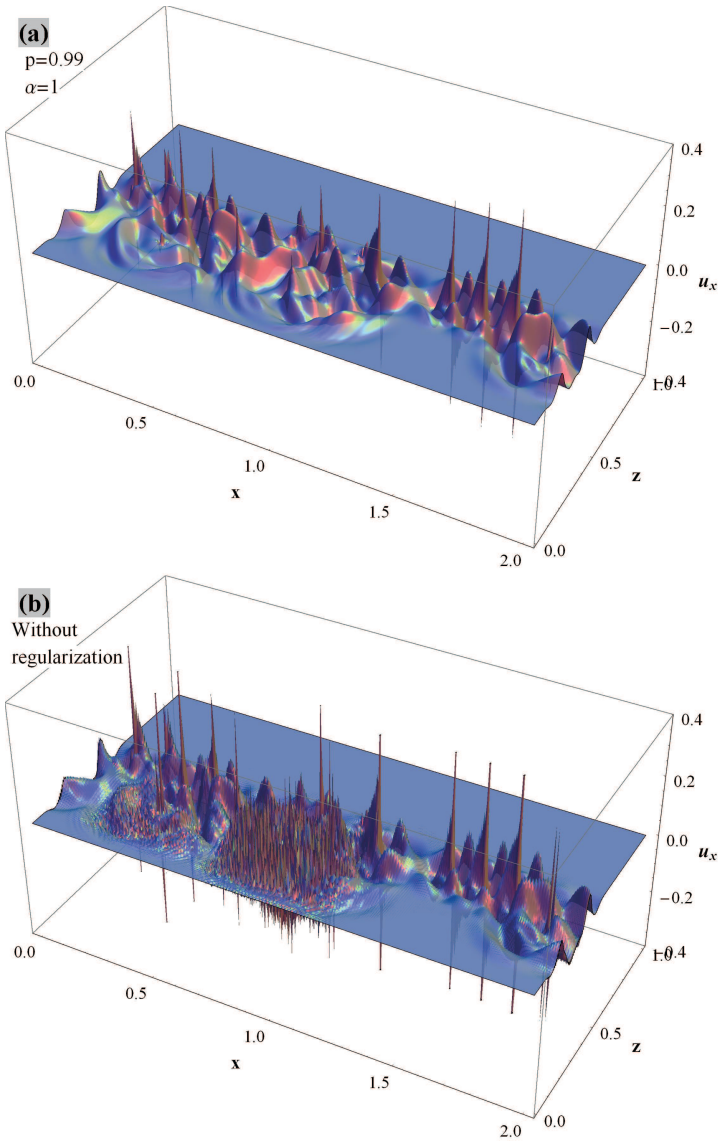

Figure 25: Snapshots of the P-SV wave propagation in a medium having fluid-filled cavities with stochastic locations; a) the solution with the regularization step with the constraint Ω_2^2; b) the solution without the regularization step.

definition is different from the classical one, described as: $\Omega_3^2=\int f''(x)^2+\alpha^2 f'(x)^2 dx$. The recently proposed definition is: $\Omega_2^2=\int (f''(x)+\alpha f'(x))^2 dx$ [30]. For this constraint, corresponding error bounds and convergence rates are qualitatively studied in this work. It is shown for the Tikhonov method with Ω_2^2 constraint, regularization can effectively control the numerical dispersion around discontinuities. To improve smoothing performance resulted from the Tikhonov methods, it is shown how to add some other favorable features,

such as conservative and local smoothing. To clarify smoothing effects of the Tikhonov method, its relationship with the filtering concept is also studied.

The proposed method can easily be extended to higher dimensions and systems of PDEs; since it is totally based on 1D algorithms. Finally to confirm efficiency of the proposed method, some 1D and 2D examples are presented. In one 1D example, the performance is compared with those of other commonly used methods developed for stress wave propagation problems. This example confirms that the performance is good and acceptable. According to another 1D benchmark, by using spatially varying regularization parameters (the adaptive regularization concept), accuracy of solutions can be improved while the Runge phenomenon can be controlled. This can be achieved, for example, by employing non-constant weights, smoothing (p) or tension (α) coefficients in the Tikhonov method. These extensions are beyond the scope of the present paper; they will be reported elsewhere.

Some 2D examples containing propagating discontinuous fronts are studied; for simulations, wave propagation in media with localized sharp transition of material properties are considered; e.g., a medium with fluid-filled crack of finite length and a medium with fluid-filled cavities with stochastic spatial locations. The results confirm that existence of even marginal regularization effects can considerably improve stability and accuracy of solutions.

Finally, it should be mentioned that one drawback of the regularization approach is proper estimation of corresponding parameters (here p and α); it seems that the trial and error method is useful to adjust proper values.

Appendix A

A.1 The Runge-Kutta 4^{th} order for stress wave problems: Second order systems

Let us assume that values of displacement ($u(t)$), velocity ($v(t):=du/dt$) and acceleration ($a(t):=d^2u/dt^2$) of a particle in motion (with spatial position x_j) are known at time $t_n:=n\Delta t$; the response at the next time step, $t_{n+1}=(n+1)\Delta t$ can be estimated by the Runge-Kutta 4^{th} order time integration as [23]:

$$\left\{u(t+\Delta t)=u(t)+\frac{\Delta t}{6}\left[v(t)+2\tilde{v}_2\left(t+\frac{\Delta t}{2}\right)+2\tilde{v}_3\left(t+\frac{\Delta t}{2}\right)+\tilde{v}_4(t+\Delta t)\right]\right\},$$
$$\left\{v(t+\Delta t)=v(t)+\frac{\Delta t}{6}\left[a(t)+2\tilde{a}_2\left(t+\frac{\Delta t}{2}\right)+2\tilde{a}_3\left(t+\frac{\Delta t}{2}\right)+\tilde{a}_4(t+\Delta t)\right]\right\},$$

where $\tilde{v}_i$ and $\tilde{a}_i$ denote guess (intermediate) velocity and acceleration at i^{th} stage, respectively; intermediate displacements, $\tilde{u}_i$ can also be defined. These guess values can be

obtained as:

$$\left\{\tilde{u}_2\left(t+\frac{\Delta t}{2}\right)=u(t)+\frac{\Delta t}{2}v(t)\right\};\qquad \left\{\tilde{v}_2\left(t+\frac{\Delta t}{2}\right)=v(t)+\frac{\Delta t}{2}a(t)\right\};$$
$$\left\{\tilde{u}_3\left(t+\frac{\Delta t}{2}\right)=u(t)+\frac{\Delta t}{2}\tilde{v}_2\left(t+\frac{\Delta t}{2}\right)\right\};\qquad \left\{\tilde{v}_3\left(t+\frac{\Delta t}{2}\right)=v(t)+\frac{\Delta t}{2}\tilde{a}_2\left(t+\frac{\Delta t}{2}\right)\right\};$$
$$\left\{\tilde{u}_4(t+\Delta t)=u(t)+\Delta t\tilde{v}_3\left(t+\frac{\Delta t}{2}\right)\right\};\qquad \left\{\tilde{v}_4(t+\Delta t)=v(t)+\Delta t\tilde{a}_3\left(t+\frac{\Delta t}{2}\right)\right\}.$$

Regarding the scalar wave equation $c^2\partial^2u/\partial x^2=\partial^2u/\partial t^2$, the equation is rewritten in a semi-discrete form: discrete in spatial domain and continuous in time. The resulted system of ODEs can then be solved by the method of lines scheme; for this, the time integration can be done by the Runge-Kutta 4^{th} order method. Let us assume the spatial discretization is done by a finite difference method at spatial location x_j; the Runge-Kutta 4^{th} order method can be implemented by considering: $u_j(t):=u(x_j,t)$, $v_j(t):=du_j/dt$ and $a_j(t):=\partial^2u_j/\partial t^2=c^2\partial^2u_j/\partial x^2$.

A.2 The generalized α-dissipative time integration method

To use this scheme, a semi-discrete form of wave equations is considered: discrete in the spatial domain and continuous in time; the spatial discretization is done with the finite element method. The semi-discrete form can then be represent as: $\mathbf{M\ddot{u}}+\mathbf{Ku}=\mathbf{F}$.

Having solution values at time step n, corresponding values at the time step $n+1$ can be obtained by the generalized α-time integration algorithm as [20]:

$$\begin{aligned}&\mathbf{F}_{n+1}=\mathbf{Ma}_{n+1}-\alpha\mathbf{Ku}_n+(\alpha+1)\mathbf{Ku}_{n+1},\\&\mathbf{u}_{n+1}=\mathbf{u}_n+\Delta t\mathbf{v}_n+\Delta t^2[(0.5-\beta)\mathbf{a}_n+\beta\mathbf{a}_{n+1}],\\&\mathbf{v}_{n+1}=\mathbf{v}_n+\Delta t[(1-\gamma)\mathbf{a}_n+\gamma\mathbf{a}_{n+1}],\end{aligned}\tag{A.1}$$

where α, β and γ are free parameters controlling the stability and numerical dissipation of the algorithm. At the initial step, we have $\mathbf{u}_0=\mathbf{u}$, $\mathbf{v}_0=\mathbf{v}$, and $\mathbf{a}_0=\mathbf{M}^{-1}(\mathbf{F}_0-\mathbf{Kd}_0)$. For case $\gamma>0.5$ numerical dissipation exists and for $\beta\geq0.25(\gamma+0.5)^2$ the mentioned algorithm is unconditionally stable [20].

A.3 The time discontinuous Galerkin method

For second order dynamical systems, the time discontinuous Galerkin method formulation can be obtained by considering the following assumptions: 1) employing the concept of the finite element method in the time domain; 2) possible existence of a discontinuity (jump) at each time step; 3) rewriting the second-order equations as first-order ones.

To account possible discontinuities, the following notations are introduced: $Z_n^{\pm}:=\lim_{\epsilon^{\pm}\to0}Z(t_n\pm\epsilon)$ and $t_n^{\pm}:=\lim_{\epsilon^{\pm}\to0}(t_n\pm\epsilon)$; where $Z\in\{\mathbf{u},\mathbf{v},\mathbf{w}_i\}$, in which: $\mathbf{w}_i:=\mathbf{w}_i(t)$

denotes a weight function and $\mathbf{v}:=\dot{\mathbf{u}}$. By considering the new variable $\mathbf{v}$, the second order (semi-discrete) equation $\mathbf{M}\ddot{\mathbf{u}}+\mathbf{C}\dot{\mathbf{u}}+\mathbf{K}\mathbf{u}=\mathbf{F}$ can be written as: $\mathbf{M}\dot{\mathbf{v}}+\mathbf{C}\mathbf{v}+\mathbf{K}\mathbf{u}=\mathbf{F}$ & $\mathbf{K}(\dot{\mathbf{u}}-\mathbf{v})=\mathbf{0}$. The weighted residual form of these first order equations on time interval $t\in[t_n^-,t_{n+1}^-]$ is [68]:

$$R_n=\int_{t_n^-}^{t_{n+1}^-}\mathbf{w}_1^T(\mathbf{M}\dot{\mathbf{v}}+\mathbf{C}\mathbf{v}+\mathbf{K}\mathbf{u}-\mathbf{F})dt+\int_{t_n^-}^{t_{n+1}^-}\mathbf{w}_2^T(\mathbf{K}(\dot{\mathbf{u}}-\mathbf{v}))dt=0,\quad \text{for } n\in\{1,\cdots,N\}, \tag{A.2}$$

where: $t_1=0$, $t_{N+1}=T$ and $t_n\le t_{n+1}$. It should be mentioned that solutions $\mathbf{u}$ & $\mathbf{v}$, and weight functions $\mathbf{w}_i$ can have discontinuities in time interval $t\in[t_n^-,t_n^+]$.

By considering linear shape functions and linear weight functions (in time domain), the following matrix form equation can be obtained from Eq. (A.2) for $t\in[t_n^-,t_{n+1}^-]$ [38]:

$$\begin{pmatrix} \frac{\mathbf{K}}{2} & \frac{\mathbf{K}}{2} & -\frac{\Delta t_n\mathbf{K}}{3} & -\frac{\Delta t_n\mathbf{K}}{6} \\ -\frac{\mathbf{K}}{2} & \frac{\mathbf{K}}{2} & -\frac{\Delta t_n\mathbf{K}}{6} & -\frac{\Delta t_n\mathbf{K}}{3} \\ \frac{\Delta t_n\mathbf{K}}{3} & \frac{\Delta t_n\mathbf{K}}{6} & \frac{\Delta t_n\mathbf{C}}{3}+\frac{\mathbf{M}}{2} & \frac{\Delta t_n\mathbf{C}}{6}+\frac{\mathbf{M}}{2} \\ \frac{\Delta t_n\mathbf{K}}{6} & \frac{\Delta t_n\mathbf{K}}{3} & \frac{\Delta t_n\mathbf{C}}{6}-\frac{\mathbf{M}}{2} & \frac{\Delta t_n\mathbf{C}}{3}+\frac{\mathbf{M}}{2} \end{pmatrix}\cdot\begin{bmatrix} \mathbf{u}_n^+ \\ \mathbf{u}_{n+1}^- \\ \mathbf{v}_n^+ \\ \mathbf{v}_{n+1}^- \end{bmatrix}=\begin{bmatrix} \mathbf{K}\mathbf{u}_n^- \\ \mathbf{0} \\ \mathbf{F}_1+\mathbf{M}\mathbf{v}_n^- \\ \mathbf{F}_2 \end{bmatrix}, \tag{A.3}$$

where $\mathbf{F}_1=\int_{t_n}^{t_{n+1}}\frac{t_{n+1}-t}{\Delta t_n}\mathbf{F}dt$ and $\mathbf{F}_2=\int_{t_n}^{t_{n+1}}\frac{t-t_n}{\Delta t_n}\mathbf{F}dt$.

A.4 Taylor-Galerkin discretizations

The second order equation of motion is again rewritten as a first order system, like: $\partial\mathbf{U}/\partial t+\partial\mathbf{E}/\partial x=\mathbf{H}$; in this equation we have: $\mathbf{U}=[\mathbf{u},\rho\mathbf{v}]^T$, $\mathbf{E}=[\mathbf{0},-\sigma]^T$ and $\mathbf{H}=[\mathbf{v},-\rho\mathbf{F}]^T$; where: σ and $\mathbf{F}$ are the stress and load vectors, respectively; and $\mathbf{v}:=\dot{\mathbf{u}}$. The momentum $\mathbf{V}=\rho\mathbf{v}$ is expanded by the Taylor series in time $t=t^n$, as: $\mathbf{V}^{n+1}=\mathbf{V}^n+\Delta t\dot{\mathbf{V}}^n+(\Delta t^2/2)\ddot{\mathbf{V}}^n+\mathcal{O}(\Delta t^3)$ (where $\mathbf{V}^n:=\mathbf{V}(t^n)$). Inserting this expansion in the first-order system, and then using the Galerkin discretization in space, the conventional (second-order) Taylor-Galerkin method can be obtained as [65]:

$$\mathbf{M}\mathbf{v}^{n+1}=\mathbf{M}\mathbf{v}^n+\Delta t\{\mathbf{H}^n-\mathbf{K}\mathbf{u}^n\}+\frac{\Delta t^2}{2}\{\dot{\mathbf{H}}^n-\mathbf{K}\mathbf{v}^n\}, \tag{A.4}$$

where $\mathbf{M}$ and $\mathbf{K}$ are the mass and stiffness matrices. Displacement $\mathbf{u}^{n+1}$ can be obtained as:

$$\mathbf{u}^{n+1}=\mathbf{u}^n+\Delta t\Big\{(1-\gamma)\mathbf{v}^n+\gamma\mathbf{v}^{n+1}\Big\}, \tag{A.5}$$

where for $\gamma=0.5$, the method is stable with maximum time step.

If a higher order Taylor expansion is used for momentum $\mathbf{V}$, a higher order Taylor Galerkin scheme can be obtained. For the third order expansion, $\mathbf{v}^{n+1}$ can be obtained

as [65]:

$$\mathbf{v}^{n+1}=\mathbf{v}^{n}+\left(\mathbf{M}+\alpha\frac{\Delta t^2}{6}\mathbf{K}\right)^{-1}\left[\Delta t\mathbf{H}^{n}+\frac{\Delta t^2}{2}\dot{\mathbf{H}}^{n}+\alpha\frac{\Delta t^2}{6}\left(\dot{\mathbf{H}}^{n-1}-\dot{\mathbf{H}}^{n}\right)\right.$$
$$\left.-\mathbf{K}\left(\frac{\Delta t^2}{2}\mathbf{v}^{n}+\Delta t\mathbf{u}^{n}\right)\right], \tag{A.6}$$

where it is needed $\alpha\geq 1/2$; for accurate solutions α near to $1/2$ should be used. For unconditional stability, it is necessary $\alpha=3/2$ and $\gamma=1/2$. Displacement $\mathbf{u}^{n+1}$ can be obtained from Eq. (A.5).

Appendix B

In this appendix, in Table 2, coefficients of generalized Padé approximations for the second derivative are presented. Coefficients of finite difference filters are provided in Table 3. For all cases, periodic boundary conditions are assumed.

Table 2: Coefficients of generalized Padé approximations for the second derivative with different accuracy and periodic boundary conditions [35].

Name	Method/order	β_2	α_2	a_2	b_2	c_2
4-C	Central/4^{th}	0	0	$\frac{4}{3}(1-\alpha_2)$	$\frac{1}{3}(-1+10\alpha_2)$	0
4-P	Padé /4^{th}	0	1/10	$\frac{4}{3}(1-\alpha_2)$	$\frac{1}{3}(-1+10\alpha_2)$	0
6-T	Tridiagonal scheme/6^{th}	0	2/11	$\frac{4}{3}(1-\alpha_2)$	$\frac{1}{3}(-1+10\alpha_2)$	0
8-C	Collatz/8^{th}	$\frac{38\alpha_2-9}{214}$	$\frac{344}{1179}$	$\frac{696-1191\alpha_2}{428}$	$\frac{2454\alpha_2-294}{535}$	0
10	10^{th}	$\frac{43}{1798}$	$\frac{334}{899}$	$\frac{1065}{1798}$	$\frac{1038}{899}$	$\frac{79}{1798}$
4-S	Spectral-like/4^{th}	0.05569169	0.50209266	0.21564935	1.7233220	0.17659730

Table 3: Filter coefficient values used for filtering the generalized Padé approximations by a post-processing stage for the periodic boundary condition [35].

Name	Method /order	$\widehat{\beta}$	$\widehat{\alpha}$	$\hat{a}$	$\hat{b}$	$\hat{c}$	$\hat{d}$
F-6-E	Explicit/6^{th}	3/10	0	1/2	3/4	3/10	1/20
F-4-T-1	Tridiagonal /4^{th}	0	0.4	$\frac{(5+6\widehat{\alpha}-6\widehat{\beta}+16\hat{d})}{8}$	$\frac{(1+2\widehat{\alpha}+2\widehat{\beta}-2\hat{d})}{2}$	$\frac{(1-2\widehat{\alpha}-14\widehat{\beta}+16\hat{d})}{-8}$	0
F-4-T-2	Tridiagonal /4^{th}	0	0.475	$\frac{(5+6\widehat{\alpha}-6\widehat{\beta}+16\hat{d})}{8}$	$\frac{(1+2\widehat{\alpha}+2\widehat{\beta}-2\hat{d})}{2}$	$\frac{(1-2\widehat{\alpha}-14\widehat{\beta}+16\hat{d})}{-8}$	0
F-4-P-1	Pentadiagonal/ 4^{th}	0.2265509	0.4627507	0.8470630	1.166845	0.3422386	0.02245659
F-4-P-2	Pentadiagonal/ 4^{th}	0.1702929	0.6522474	0.9891856	1.321180	0.3333548	0.001359850

References

[1] D. Appelö, J. W. Banks, W. D. Henshaw, and D. W. Schwendeman, 2012: Numerical methods for solid mechanics on overlapping grids: Linear elasticity, J. Comput. Phys., 231(18), 6012-6050.

[2] R. Arcangeli, and B. Ycart, 1993: Almost sure convergence of smoothing D^m-splines for noisy data, Numer. Math., 66(3), 281-294.

[3] J. W. Banks, and W. D. Henshaw1, 2012: Upwind schemes for the wave equation in second-order form, J. Comput. Phys., 231(17), 5854-5889.

[4] V. Barakat, B. Guilpart, R. Goutte, and R. Prost, 1997: Model-based Tikhonov-Miller image restoration, IEEExplore, Proceedings International conference on Image processing (ICIP '97), pp. 310-31, ISBN: 0-8186-8183-7, Washington, DC, USA, October 26-29.

[5] F. Boulsina, M. Berrabah, and J. C. Dupuy, 2008: Deconvolution of SIMS depth profiles: Towards simple and faster techniques, Appl. Surf. Sci., 255(5), 1946-1958.

[6] J. P. Boyd, 1992: Defeating the Runge phenomenon for equispaced polynomial interpolation via Tikhonov regularization, Appl. Math. Lett., 5(6), 57-59.

[7] J. P. Boyd, and J. R. Ong, 2009: Exponentially-convergent strategies for defeating the Runge phenomenon for the approximation of non-periodic functions, Part I: Single-interval schemes, Commun. Comput. Phys., 5(2-4), 484-497.

[8] M. Calhoun-Lopez, and M. D. Gunzburger, 2005: A finite element, multiresolution viscosity method for hyperbolic conservation laws, SIAM J. Num. Anal., 43, 1988-2011.

[9] M. Calhoun-Lopez, and M. D. Gunzburger, 2007: The efficient implementation of a finite element, multi-resolution viscosity method for hyperbolic conservation laws, J. Comput. Phys., 225, 1288-1313.

[10] R. Chartrand and V. Staneva, 2008: Total variation regularization of images corrupted by non-Gaussian noise using a quasi-Newton method, IEEE T. Image Processing, 2(6), 295-303.

[11] J. Cullum, 1971: Numerical differentiation and regularization, SIAM J. Num. Anal., 8(2), 254-265.

[12] S. M. Day, and G. P. Ely, 2002: Effect of a shallow weak zone on fault rupture: Numerical simulation of scale-model experiments, Bull. Seismol. Soc. Am., 92(8), 3022-3041.

[13] S. M. Day, L. A. Dalguer, N. Lapusta, and Y. Liu, 2005: Comparison of finite difference and boundary integral solutions to three-dimensional spontaneous rupture, J. Geophys. Res., 110.

[14] B. Fornberg, 1998: Calculation of weights in finite difference formulas, SIAM Rev. 40(3), 685-691.

[15] B. Gautier, G. Prudon, and J. C. Dupuy, 1998: Toward a better reliability in the deconvolution of SIMS depth profiles, Surf. Interface Anal., 26(13), 974-983.

[16] D. Gottlieb, and J. S. Hesthaven, 2001: Spectral methods for hyperbolic problems, J. Comput. Appl. Math., 128(1-2), 83-131.

[17] C. W. Groetsch, 1998: Lanczo's generalized derivative, Amer. Math. Monthly, 105, 320-326.

[18] Y. Gu, and G. W. Wei, 2003: Conjugate filter approach for shock capturing, Commun. Numer. Meth. Engng, 19, 99-110.

[19] P. C. Hansen, 1998: Rank-Deficient and Discrete Ill-Posed Problems, Philadelphia: SIAM.

[20] H. M. Hilber, T. J. R. Hughes, and R. L. Taylor, 1977: Improved numerical dissipation for time integration algorithms in structural dynamics, Earthq. Eng. Struct. Dyn., 5(3), 283-292.

[21] C. Hoff, and P. J. Pahl, 1988: Development of an implicit method with numerical dissipation from a generalized single step algorithm for structural dynamics, Comput. Methods Appl.

Mech. Eng., 67(3), 367-385.
[22] C. Hoff, and P. J. Pahl, 1988: Practical Performance of the θ1- method and comparison with other dissipative algorithms in structural dynamics, Comput. Methods Appl. Mech. Eng., 67, 87-110.
[23] W. G. Hoover, 2006: Smooth Particle Applied Mechanics, The State of the Art, Word Scientific.
[24] B. K. P. Horn, and B. G. Schunck, 1981: Determining optical flow, Artificial Intelligence, 17(1-3), 185-203.
[25] T. J. R. Hughes, 1987: The Finite Element Method: Linear Static and Dynamic Finite Element Analysis, Englewood Cliffs: Prentice Hall.
[26] G. H. Hulbert, and J. Chung, 1996: Explicit time integration algorithms for structural dynamics with optimal numerical dissipation, Comput. Methods Appl. Mech. Eng., 137, 175-188.
[27] M. F. Hutchinson, and F. R. de Hoog, 1985: Smoothing noisy data with spline functions, Numer. Math., 47(1), 99-106.
[28] F. Jauberteaua, and J. L. Jauberteaub, 2009: Numerical differentiation with noisy signal, Appl. Math. Comput., 215(6), 2283-2297.
[29] J. Kawahara, and T. Yamashita, 1992: Scattering of elastic waves by a fracture zone containing randomly distributed cracks, Pure Appl. Geophys., 139, 121-144.
[30] S. N. Kersey, 2006: Mixed interpolating-smoothing splines and the ν-spline, J. Math. Anal. Appl., 322(1), 28-40.
[31] I. R. Khan, and R. Ohba, 2000: New finite difference formulas for numerical differentiation, J. Comput. Appl. Math., 126, 269-276.
[32] A. Kurganov, and M. Pollack, 2011: Semi-discrete central-upwind schemes for elasticity in heterogeneous media, (submitted for publication).
[33] C. Lanczos, 1956: Applied Analysis, Prentice-Hall, Englewood Cliffs, NJ.
[34] T. Le, R. Chartrand, and Th. J. Asaki, 2007: A variational approach to reconstructing images corrupted by Poisson noise, J. Math. Imaging Vision, 27(3), 257-263.
[35] S. K. Lele, 1992: Compact finite difference schemes with spectral-like resolution, J. Comput. Phys., 103(1), 16-42.
[36] T. C. M. Lee, 2003: Smoothing parameter selection for smoothing splines: A simulation study. Comput. Stat. Data Anal., 42(1-2), 139-148.
[37] R. J. LeVeque, 1992: Numerical Methods for Conservation Laws, second edition, Berlin, Birkhäuser.
[38] X. D. Li, and N. E. Wiberg, 1996: Structural dynamic analysis by a time-discontinuous Galerkin finite element method, Int. J. Numer. Methods Eng., 39, 2131-2152.
[39] C. Loader, 2004: Smoothing: Local regression techniques, in J. E. Gentle, W. Härdle, and Y. Mori, Hand-Book of Computational Statistics Concepts and Methods, Berlin: Springer.
[40] G. Nakamura, S. Wang, and Y. Wang, 2008: Numerical differentiation for the second order derivatives of functions of two variables, J. Comput. Appl. Math., 212, 341-358.
[41] Y. P. Petrov, and V. S. Sizikov, 2005: Well-Posed, Ill-Posed, and Intermediate Problems with Applications, Berlin, Boston: De Gruyter.
[42] S. Pruess, 1976: Properties of splines in tension, J. Approx. Theory, 17(1), 86-96.
[43] S. Pruess, 1978: An algorithm for computing smoothing splines in tension, Computing, 19(4), 365-373.
[44] D. L. Ragozin, 1983: Error bounds for derivative Estimates based on spline smoothing of exact or noisy data, J. Approx. Theory, 37, 335-355.
[45] A. G. Ramm, and A. B. Smirnova, 2001: On stable numerical differentiation, Math. Comp.,

70(235), 1131-1153.
[46] A. G. Ramm, and A. Smirnova, 2003: Stable numerical differentiation: When is it possible?, Jour. Korean SIAM, 7(1), 47-61.
[47] S. K. Rangarajana, and S. P. Purushothaman, 2005: Lanczo's generalized derivative for higher orders, J. Comput. Appl. Math., 177, 461-465.
[48] P. Rentrop, 1980: An algorithm for the computation of the exponential spline, Numer. Math., 35(1), 81-93.
[49] P. Rentrop, and U. Wever, 1987: Computational strategies for the tension parameters of the exponential spline, in M. Thoma, F. Allgöwer, and M. Morari, Lecture Notes in Control and Information Sciences, Springer: ISSN: 0170-8643, pp 122-134.
[50] P. Rodríguez, 2013: Total variation regularization algorithms for images corrupted with different noise models: A review, J. Electr. Comput. Engrg, 2013, 1-18.
[51] T. Rohlfing, C. R. J. r. Maurer, D. A. Bluemke, and M. A. Jacobs, 2003: Volume-preserving nonrigid registration of MR breast images using free-form deformation with an incompressibility constraint, IEEE T. Med Imaging, 22(6), 730-41.
[52] D. Ruan, J. A. Fessler, M. Roberson, J. Balter, and M. Kessler, 2006: Nonrigid registration using regularization that accomodates local tissue rigidity, Proc. SPIE 6144, Medical Imaging 2006: Image Processing, 614412; doi:10.1117/12.653870.
[53] L. I. Rudin, S. Osher, and E. Fatemi, 1992: Nonlinear total variation based noise removal algorithms, Physica D (Nonlinear Phenomena), 60(1-4), 259-268.
[54] M. C. L. de Silanes, 1997: Convergence and error estimates for (m,l,s)-splines, J. Comput. Appl. Math., 87(2), 373-384.
[55] J. Sochacki, R. Kubichek, J. George, W. R. Fletcher, and S. Smithson, 1987: Absorbing boundary conditions and surface waves, Geophysics, 52(1), 60-71.
[56] E. Tadmor, 1989: Convergence of spectral methods for nonlinear conservation laws, SIAM J. Num. Anal., 26(1), 30-44.
[57] D. Terzopoulos, 1986: Regularization of inverse visual problems involving discontinuities, IEEE T. Pattern Anal. Mach. Intell., 8(4), 413 - 424.
[58] J. A. Trangenstein, 2007: Numerical Solution of Hyperbolic Partial Differential Equations, Cambridge University Press, New York.
[59] J. Walden, 1999: Filter bank methods for hyperbolic PDEs, SIAM J. Num. Anal., 36(4), 1183-1233.
[60] Y. Wang, X. Jia, J. Cheng, 2002: A numerical differentiation method and its application to reconstruction of discontinuity, Inverse Probl., 18, 1461-1476.
[61] Z. Wang, and R. Wen, 2010: Numerical differentiation for high orders by an integration method, J. Comput. Appl. Math., 234(3), 941-948.
[62] G. W. Wei, and Y. Gu, 2002: Conjugate filter approach for solving Burgers equation, J. Comput. Appl. Math., 149, 439-456.
[63] T. Wei, Y. C. Hon, Y. Wang, 2005: Reconstruction of numerical derivatives from scattered noisy data, Inverse Probl., 21, 657-672.
[64] K. Yomogida, and R. Benites, 2002: Scattering of seismic waves by cracks with the boundary integral method, Pure Appl. Geophys., 159, 1771-1789.
[65] S. K. Youn, and S. H. Park, 1995: A new direct higher-order Taylor-Galerkin finite element method, Comput. & Structures, 56(4), 651-656.
[66] H. Yousefi, A. Noorzad, and J. Farjoodi, 2010: Simulating 2D waves propagation in elastic solid media using wavelet based adaptive method, J. Sci. Comput., 42(3), 404-425.
[67] H. Yousefi, A. Noorzad, and J. Farjoodi, 2013: Multiresolution based adaptive schemes for

second order hyperbolic PDEs in elastodynamic problems, Appl. Math. Modell., 37(12-13), 7095-7127.

[68] O. C. Zienkiewicz, and R. L. Taylor, 2000: The Finite Element Method, Volume 1, The Basis, John Wiley & Sons Canada, Ltd., 5th edition.

[69] D. W. Zingg, H. Lomax, and H. Jurgens, 1996: High-accuracy finite-difference schemes for linear wave propagation, SIAM J. Sci. Comput., 17(2), 328-346.

[70] D. W. Zingg, 2000; Comparison of high-accuracy finite-difference methods for linear wave propagation, SIAM J. Sci. Comput., 22(2), 476-502.